2019-11-01

Hydrological and Paleoclimate Analysis of a Pinyon-Juniper and Fen-Dominated Watershed on the Windy Ridge Mega-Landslide

Joel Frederick Barker
Brigham Young University

Hydrological and Paleoclimate Analysis of a Pinyon-Juniper and Fen-Dominated Watershed on the Windy Ridge Mega-Landslide

Joel Frederick Barker

A thesis submitted to the faculty of
Brigham Young University
in partial fulfillment of the requirements for the degree of

Master of Science

Stephen Nelson, Chair
Sam Hudson
Barry Bickmore

Department of Geological Sciences

Brigham Young University

ABSTRACT

Hydrological and Paleoclimate Analysis of a Pinyon-Juniper and Fen-Dominated Watershed on the Windy Ridge Mega-Landslide

Joel Frederick Barker
Department of Geological Sciences, BYU
Master of Science

Chapter 1: Water Budget

This chapter documents the hydrologic analysis of a watershed within the Windy Ridge mega-landslide of Central Utah to (1) create a water budget and (2) place a quantitative limit on the magnitude of climatic changes documented by Shurtliff et al. (2017) and Hudson et al. (2019).

(1) A water budget was calculated over the last four years using instrumentation and weather stations both within and surrounding the watershed, In terms of precipitation input, 85% is released by the evapotranspiration of the Pinyon-Juniper forest, 4% discharges as surface water from the base of the watershed, and 11 % infiltrates the groundwater system. This infiltration rate is slightly lower than the 15% suggested by Maxey-Eakin method (Maxey and Eakin, 1949), likely due to the less permeable, clay-rich sediment.

(2) Previous studies performed on Garden Basin Cattail (GBC) Fen at the base of its watershed suggest swings from pond-like to wetland environments (Shurtliff et al, 2017; Hudson et al, 2019). This study estimated precipitation values necessary to create standing water (pond) environments.

Changes in annual precipitation, as well as input from North American monsoon (NAM), may cause these environmental changes. Each of these cases were examined. Trends in piezometer measurements compared to mean annual precipitation indicated that $\geq$ 644 mm of annual precipitation are required to sustain a wet (perennial standing water) environment. The change from wetland to pond conditions may depend on seasonal trends in precipitation. This study suggests an increase of 150-300 mm of precipitation in late summer (NAM) may be connected to perennially wet conditions. The higher annual precipitation values, largely accomplished by NAM fluctuations, caused a transition from wetland to pond (Hudson et al., 2019; Shurtliff et al., 2017).

Chapter 2: Core Analysis

Chapter 2 further documents the watershed's historical environmental and climate record by analyzing sediment and topography surrounding GBC fen, adding to the works of Shurtliff et al. (2019) and Hudson et al. (2019). A core was extracted from GBC fen at the base of the watershed and the sediment analyzed in terms of color, texture, environmental scanning electron microscope (ESEM) imaging, RockEval pyrolysis, and ^{14}C ages. These results were then compared to pre-existing pollen and diatom proxies completed on a previous core by Shurtliff et al. (2019). This study suggests climatic variation, along with basin fill processes, was the driver of environmental change in GBC fen (Garden Basin watershed). Climate proxies show the basic

trend from a particularly wet period (12-9 ka BP) of more stagnant or deeper water, to a much dryer period of much shallower water levels (9-3 ka BP), followed by a rebound in moisture levels, especially in the past few hundred years. Although climate was the driver of transitions within GBC2 core, a pollen record of sustained shallow water plants and MASW survey (Park et al., 1999) suggest beaver activity.

Keywords: water budget, evapotranspiration, climate, weather station, piezometer, hydrograph, transpiration, outflow, precipitation, pyrolysis, radiocarbon ages, core description, pollen

ACKNOWLEDGEMENTS

This study is a continuation of the research and effort by Shurtliff et al. (2014) who was able to use pollen identification to create a paleoclimate record of the area. My mentor Dr. Stephen Nelson was a great source of knowledge, support, and experience. I must mention the other members of my thesis committee, Barry Bickmore and Sam Hudson, for their research assistance and technical expertise. Greg Carling was integral in creating a water budget and understanding the hydrology of the area.

Kevin Rey was key in accompanying me to the Garden Basin Cattail Fen multiple times, teaching me the intricacies of our monitoring equipment, and helping me in every step of the coring process. Dave Tingey was essential in creating a survey of the area and setting up the flume at the spill point. Most importantly, my wife must be acknowledged for her love and patience throughout the entire thesis process.

TABLE OF CONTENTS

CHAPTER 1: WATER BUDGET

INTRODUCTION

A water budget quantifies the balance between water flowing into and out of a watershed, and can be a great tool in determining the availability and sustainability of a local water supply (Healy, 2007). Water is becoming a more precious resource in the Western United States, with some scientists predicting massive drops in precipitation for the west in the near future due to climate change (NASA, 2015; Cook et al., 2015), driving the need to develop accurate water budgets for watersheds throughout the Western United States.

This chapter focuses on the construction of a water budget for Garden Basin watershed located in the Geyser Peak 7 ½' Quadrangle of central Utah (Nelson, 1989). Calculating a water budget for this watershed required the measurement of water inputs and outputs. A variety of data sources were used to calculate water flow, including a weather station, piezometers, flow meters, MATLAB interpolation tools, thermistors, a trail camera, coring equipment, and near infrared satellite images. The interpretation of the data from these instruments show the balance between the flow of water into the watershed (precipitation) and its methods of removal (evapotranspiration, infiltration, and runoff).

The watershed has unique hydrologic characteristics due to its location atop the Windy Ridge mega-landslide (Fig. 1.1). The landslide's hummocky topography provided basins for the fens that dot the watershed (Shurtliff et al., 2017). Of special interest was the GBC fen located at the base of the watershed, being the terminal point for flow accumulation.

The required precipitation for these environments was calculated for two cases: (1) A change in annual precipitation values and (2) fluctuations in monsoonal summer rains or North American monsoon (NAM).

Previous Studies

GBC fen has been studied by both Shurtliff et al. (2014; 2017) and Hudson et al. (2019). These studies document the direction of climatic change over the past ~12,000 yr., focusing on changes from pond-like to more wetland environments (Shurtliff et al., 2017: Hudson et al., 2018). This study focuses on determining the magnitude of change between these states, specifically the precipitation values necessary to sustain these endmember environments.

Purpose and Objectives

The purpose of this study is to estimate the change in precipitation needed to maintain perennial standing water in the GBC fen by (1) perform a water balance study on the watershed and (2) calculating the precipitation necessary to sustain a pond environment. This will place limits to the magnitude of precipitation needed to produce the environmental change documented by Shurtliff et al. (2017) and Hudson et al. (2019).

Hydrologic and Geologic Setting

The Garden Basin watershed resides on the Windy Ridge mega-landslide of the Thousand Lake landslide zone (Nelson, 1989; Fig. 1.1). The Windy Ridge mega-landslide developed in the weak shale layers of the Brushy Basin Member of the Morrison Formation during late Pleistocene to Holocene time (Shurtliff, 2014; Fig. 1.2). The slide slipped down dip along the east-dipping limb of the Thousand Lake Anticline (Nelson, 1989).

This watershed encompasses ~990,000 m^2 of Pinyon-Juniper forest, interspersed with grasslands and wetlands. These fens likely contain standing water for about one third of the year according to water level monitoring of the GBC fen documented below. The GBC fen represents a terminal point in its small watershed during the late summer and fall when surface water does not spill. This is due to the fen occupying a small endorheic basin (swale) between hummocks of

the landslide. However, most of these fens are connected to others by small channels.

Infiltration rates within the watershed are thought to be low due to the fine clays of the Brushy Basin Member of the Morrison Formation. These fine clays effectively fill the interstices between tertiary volcanic clasts (Fig. 1.3), and create a relatively impervious boundary (Bear, 1972), reducing the infiltration rate of precipitation. The landslide matrix is composed of Brushy Basin Member clays that were mechanically mixed with volcanic rocks that cap undisturbed bedrock at the breakaway zone. Thus, the matrix has a low permeability (Nelson, 1989; Bear, 1972).

Precipitation is affected by the prevailing SW-NE winds flowing over the ridge to the west (Fig. 1.1 & 1.2) as documented later in this study. This flow likely creates a rain shadow over the Garden Basin. Due to the close proximity of the watershed to the northern limit of the modern North American monsoon (NAM) (Grantz et al., 2007), the influence of past monsoonal precipitation was closely examined.

METHODS

This section describes the methods to arrive at input values for each variable in the water budget. Due to the large amount of data collected and the complexity of the setting, this section requires more detail than is often necessary.

Field Instrumentation

Surveying: In order to obtain the most precise geometries possible for critical feature, especially elevations, a total station surveying system was later used to document small elevation changes of the fen surface and especially the difference in elevation between the depocenter and the spill point elevation on the adjacent sill.

Water Level Measurements: During the typical year, water levels vary from above to

below ground. In order to track changes in the potentiometric surface, a 5.1 cm diameter PVC piezometer was installed near the depocenter (within the cattail stand; Fig. 1.4). The base was screened and packed with sand and the top was sealed with bentonite. The piezometer was instrumented with three HOBO U20 pressure transducers that recorded pressures every one to six hours. One transducer was placed above ground in the PVC stickup to enable water level corrections due to barometric pressure changes (HOBO, 2019). Table 1 records well dimensions and transducer position.

Soil Temperature Measurements: Monitoring soil temperature is useful for detecting the timing of snowmelt and the photosynthetic activity of PJ forest. When snow is melting, soil temperatures are buffered to 0°C in the presence of liquid and solid water, and when soil temperatures drop below 4.4°C, water uptake at the root surface significantly decreases (Miller, 2005). Soil temperatures in landslide material surrounding the GBC fen were monitored using Maxim Integrated thermistors (DS1922L). They were nested at various depths in order to monitor differences between diurnal and seasonal temperature variations.

Weather Station: In order to calculate evapotranspiration (ET) on the fen as well as assessing local precipitation rates, A Davis weather station using Weatherlink software was installed at a height of 2.4 m above ground surface to a 9.1 x 9.1 cm wooden post near the piezometer (Fig. 1.5). Wind speed and direction, temperature, precipitation, humidity, and solar radiance were logged over a 4 year period, enabling the Penmann-Montieth ET values to be calculated (Allen et al., 1998).

Trail Camera: A Windsong trail camera was installed to a metal fence post east of the piezometer (Fig. 1.5). This allowed monitoring of standing-water depth on the fen as well as the depth duration of snowfall and snowpack. Unfortunately, the photographic record is incomplete

due theft of the camera.

Weir: In order to better quantify water fluxes when the GBC fen was spilling, a 20.3 cm horizontal PVC pipe was placed below the spill point to channel all water spilling from the fen though it. The pipe was embedded in bentonite to minimize underflow and packed with. The pipe was buried in bentonite clay to prevent underflow and packed with additional sand and rock. For the 2018-2019 water year, the trail camera was position near the pipe outflow in order to monitor water fluxes with time, using the equation for a circular weir. Unfortunately, the SD memory card was stolen. However, hard water deposits within the pipe were used to determine sustained water heights, which could be used to estimate flows.

Water Budget

Water Budget Equation: Given the similarity in the hydrogeological setting, an approach similar to Riddell et al. (2013) was used to evaluate the hydrology of the GBC fen watershed:

$$P + GW_{in} = ET + Q + I + GW_{out} \quad (1)$$

$$P = precipitation\ over\ the\ GBC\ fen\ drainage\ basin$$
$$GW_{in} = groudwater\ flow\ into\ the\ GBC\ drainage\ basin$$
$$ET = evapotranspiration\ from\ the\ GBC\ drainage\ basin$$
$$Q = surface\ water\ outflow\ from\ the\ GBC\ fen$$
$$I = infiltration\ (recharge)\ to\ the\ GBC\ drainage\ basin$$
$$GW_{out} = groundwater\ flow\ out\ of\ the\ GBC\ drainage\ basin$$

If a steady-state condition flow conditions are assumed for groundwater, Eq. 1 reduces to:

$$P = ET + Q + I \quad (2)$$

Precipitation: P is a fundamental variable in the water balance approach, and various methods of estimating it over the GBC drainage basin will produce somewhat different results. Thus, four methods were used to estimate P and are evaluated in the Discussion in terms of their impact to the water budget. Although a preferred approach is adopted, all four methods are considered in order to evaluate the consequences of adopting a particular approach. The four methods are:

- Precipitation values from the weather station were applied to the entire drainage basin. As the weather station is at the lowest elevation within the area, orographic influence may be underestimated. In addition, the tipping bucket rain gauge may not record all precipitation received as snow.
- 30-year average PRISM (2019) 800 m precipitation data were used. A potential weakness of this approach is that for the GBC drainage area, precipitation rates are interpolated from records of surrounding weather stations.
- Interpolation of precipitation data from the 10 nearest weather stations to the GBC fen using algorithms in MATLAB.
- Similar to Maxey and Eakin (1949), an empirical relationship was established using elevation and historical precipitation using nearby weather stations. This permits an interpolated estimate of precipitation based on the elevation of the GBC drainage. A

problem with this approach is that the GBC area is in a rain shadow, such that true precipitation may be overestimated.

Evapotranspiration: Goulden et al. (2012) presented an empirical relationship between ET determined by flux tower measurements and normalized difference vegetation index (NDVI) measurements over a wide-range of elevations and plant communities that are similar the GBC catchment. As such, we apply this approach to estimate ET for PJ forest. The expression of Goulden et al., (2012) is:

$$ET = 101.49\left[e^{(2.6853xNDVI)}\right] \quad (3)$$

NDVI data of 250 x 250 m resolution was obtained from NASA (2019) extending from 2015 to 2018. NDVI data are also used to evaluate the timing and relative vigor of ET over time.

The goal of this study is to generate a water budget that evaluates the GBC fen in its current state, but with pristine vegetation surrounding it. However, the GBC watershed has been modified by the partial removal of PJ forest, converting 30% of the area into rangeland for cattle. Data from both USGS (2018) and NASA (2019) show a drastically lower NDVI values (28% and 54%) for rangelands devoid of pinyon-juniper (Fig. 1.6). To remove the effect of anthropogenic destruction of PJ forest, NDVI values from a pixel of forest (devoid of rangeland) from the watershed was assumed to indicate pristine vegetation conditions. Further comparison of values was performed on a pixel containing PJ forest versus a pixel containing rangeland.

In addition to rangeland, the GBC watershed is also occupied by wetlands (Fig. 1.1 and 1.4, accounting for 4.9% of the area. Like the GBC fen, many of these are filled with standing water at least part of the year, and the NDVI approach (Goulden et al., 2012) will underestimate ET for areas dominated by evaporation. To account for this, pan evaporation was estimated as a surrogate following the method of Doorenbos (1977) along with data and ET estimates from from the weather station, where:

$$ET_{pan} = ET_{ws}/K_p \quad (4)$$

$$ET_{pan} = estimated\ pan\ evaporation$$
$$ET_{ws} = reference\ ET\ from\ the\ weather\ station$$
$$K_p = pan\ coefficient$$

$$ET_a = 0.049\left[fxET_{pan} + (1-f)ET_{ws}\right] + ET_{NDVI} - 0.049ET_{NDVI} \quad (5)$$

$$0.0490 = fraction\ of\ GBC\ watershed\ occupied\ by\ wetlands$$
$$f = fraction\ of\ days\ of\ standing\ water\ in\ GBC\ fen$$
$$ET_{ws} = ET\ estimated\ from\ the\ weather\ station$$
$$ET_{NDVI} = ET\ estimated\ assuming\ no\ rangeland$$
$$ET_a = Actual\ ET$$

Pinyon-Juniper Transpiration: As a check on calculated evapotranspiration values, aerial imagery was used to calculate the number of trees in 3 photos of 55 m x 34 m resolution (Google Earth, 2015) within the pinyon-juniper forest. MATLAB software was used to calculate the area of PJ canopy within each image. The areas of 6 single, adult trees were averaged to assume the average canopy area of a single PJ tree. The overall canopy area was divided by the value of a single tree to estimate the total number trees in each image. This value was divided by the resolution of the images to calculate a tree density for the watershed. The measured density (tree per m^2) was then multiplied by the area of the watershed (~990,000 m^2) for an estimation of the total number of trees within the watershed. The number of trees was multiplied by the estimated transpiration rates of pinyon/juniper trees suggested in the literature (Bedell, 1993; De Rocher et al., 1993) for an estimate of the pinyon-juniper forest's yearly transpiration potential.

Surface Outflow: Given the remote nature of the GBC fen, it was not possible to regularly monitor outflows from the circular weir. As noted above, efforts to use a trail camera to measure water depths were unsuccessful, and water depths in the pipe were too shallow and irregular to make monitoring with a pressure transducer possible. As a result, two other approaches were used for estimating outflow. First, the natural spill point has a nearly rectangular cross section permitting fluxes to be measured with a flow meter when the GBC fen was visited while spilling. Second, hard water deposits on the inside of the PVC pipe indicated water depths indicative of prolonged flow (Fig. 1.7).

Seepage: Seepage was treated as part of the surface outflow term in the water budget. It occurs at several points where groundwater emerges from the fen sill-barrier system several m south of the spill point and 0.6 to 0.9 m lower in elevation (Fig. 1.8). This seepage converges into a single small channel with a roughly rectangular cross section where flux could also be

measured with a flow meter. Annual seepage was estimated by multiplying fluxes by the number of days the fen contained standing water as indicated by piezometer data. Both spill and especially the seepage terms are small relative to the P, ET, and I such that their larger uncertainties contribute relatively little error to the total budget.

RESULTS

Field Instrumentation

Surveying: The survey (Fig. 1.9; Appendix) provided critical geometric relations to understand the max depth of standing water, how flat the fen is, thresholds for the hydrograph discussed below, etc. For example, it revealed that the fen would only need to fill to 0.32 m (1.03 feet) above the fen surface in order to reach the spill point.

Water Level Measurements: After correcting for barometric effects, the piezometer measurements can be shown as water levels in comparison to the ground level, spill point, and seepage areas (water levels seen in Fig. 1.10; positions seen in Fig. 1.9). Piezometer data show that water begins to rise mid-winter, then decline during late summer and fall. The plateaus in the data signify the spillage of the fen from mid-winter to mid-summer and average to about 135 days of spill and 214 days of standing water per year. There is a sharp rise and fall between each of these periods. Figure 1.11 shows the relationship between evapotranspiration and piezometer measurements, like quasi-sinusoidal trends out of sync.

There were a few unrealistic spikes and declines in apparent water levels around the end of February in multiple years. Increased pressure may be due to ice formation in the piezometer, whereas the dips remain unexplained. These outlying peaks and troughs were ignored in this study.

Soil Temperature Measurements: The average soil temp at 10 cm was about 8.6°C and

ranges from 28 °C in summer to -5 °C in the winter. Deeper thermistors show that soil temperature reacts less to diurnal variations with depth. Although mean annual temperature under the surface stays constant at different depths, the difference between maximum and minimum yearly temperatures decreases with depth (Fig 1.12). Analysis of soil temperatures versus NDVI (or ET; Fig. 1.13) measurements depict a sharp rise in water levels during the coldest annual soil temperatures.

Weather Station: The Davis weather station recorded precipitation and wind speed/direction measurements every two hours. A rose diagram from these records shows a prevailing ENE wind direction (Fig. 1.14). The analysis of precipitation values against water level rise (groundwater recharge) from the hydrograph (Fig. 1.15) enabled specific yield calculations. One rain event (Figure 1.15) analyzed for recharge and water table rise. The specific yield from the event came to 27.2%. It is hypothesized the calculated values of specific yield are due to the mixture of multiple sediment types including peat (44%), volcanic gravel (21), and clay (6) (Morris and Johnson, 1967). The maximum water dip in autumn is ~63 cm from 2014 to 2018. Eq. 6 (Nimmo et al., 2015, Zhang et al., 2017) was used to solve for recharge (R):

$$R = Sy \times H \quad (6)$$

Sy = specific yield

H = the rise (m) in the water table corresponding to the event

R = recharge (m)

Added precipitation of ~230 mm during late fall may increase the water table above the GBC fen depocenter.

Trail Camera: Images of the fen showed that snow levels rose during snow events.

However, the snow melted very quickly, likely adding height to the water table and/or the height of water within the fen.

Weir and Seepage: Two methods were used to estimate the amount of water leaving the fen. Figure 1.16 [A & B] depicts the dimensions and flow velocity of water leaving the fen from natural flow channels. Figure 1.7 shows the height of water based on hard water deposits within the pipe, ~38 mm, which was used to calculate spillage through Eq. 3 and 4. Total yearly outflow of each method of spillage estimation were averaged and added to seepage to calculate an average 16,676 m^3/yr. (Table 2; Refer to Appendix for calculations) of water lost from GBC fen based on 2/2/2017 to 11/3/2017 weir data.

Water Budget

Precipitation: Multiple methods were used to estimate annual precipitation. A spline interpolation of surrounding COOP weather stations was coded in Matlab (Fig. 1.17). This interpolation shows a large dip in precipitation levels from west to east and estimated a precipitation rate of 381 mm/yr. in Garden Basin. Thirty year averages were found using PRISM (PRISM, 2019) from Oregon State University at a resolution of 800m. This calculated yearly precipitation averages of about 380 mm as well.

The Maxey-Eaken method was then used to compare elevation to precipitation measured from COOP weather stations in Central Utah (Maxey and Eakin, 1949). The trend suggests about 420 mm at the elevation of our fen: 2450 m. Finally, the weather station located in the fen measured precipitation from late 2014 to mid-2018 and calculated about 372 mm/yr. These four methods come to some fairly comparable results that will be discussed further later in this study.

Evapotranspiration: Evapotranspiration was calculated by inserting NDVI values into Eq. 3. The average yearly evapotranspiration from this NDVI comes to 273 mm/year (NASA, 2019;

Fig. 2.6). The weather station located within the fen calculated a yearly reference evapotranspiration (suggesting a green cropped area) of about 1162 mm/yr., which is not far from the trend of other weather stations in the area which experience between 800 and 1200 mm/yr. depending on elevation. Eq. 4 and 5 were used to correct for the original evapotranspiration estimate [from NDVI] for the higher evapotranspiration of fens. This produced an actual evapotranspiration value of 324 mm/yr from 2015 to 2018, assuming that the wetlands (like GBC fen) contain standing water about half of the year (Fig. 1.10). Further analysis showed that ET values of rangeland is 28% to 35% lower in rangeland (NASA, 2019; USGS, 2018; Eq. 3), which correlates to ~2.5% loss in ET for every 10% of PJ forest lost.

Figure 1.18 shows the flow vectors of evapotranspiration, discharge, and infiltration in terms of precipitation.

Pinyon-Juniper Transpiration: Although estimating water consumption of pinyon and juniper trees in different environments can be difficult, values were constrained from literature. Bedell (1993) suggests that western junipers use 75,000 to 150,000 ml of water per day depending on environmental conditions. The period of decline in the water table data suggest an average of 94 days of water table decline below the fen's surface each year. Tree density calculations estimate that ~22,000 trees exist within the watershed, taking up between 156 and 313 mm/yr of water during the subsurface water table decline. In other words, ~150 to 300 mm/yr of added precipitation during this period may produce pond conditions (water level above the fen surface) all year long. Further analysis of the total duration of negative slope indicates that between 270 and 540 mm/yr of added precipitation could cause continuous spilling all year. But, if the GBC fen did not spill, the water level readings during spill time may theoretically resemble a hyperbolic rise and fall. This would suggest an added 68 days of decline, which brings the total

decline to 228 days. Considering that the density of trees within this PJ forest is about 45 m^2 per tree, the PJ forest likely transpires between 381 and 763 mm each year assuming pristine conditions. These estimates start just above the current 380 mm/yr value of modern precipitation (PRISM, 2018).

DISCUSSION

Water Budget

The water budget for the GBC watershed was simplified to just the variables precipitation, evapotranspiration, infiltration to groundwater, and surface outflow (Eq. 2). This is possible because the chief input to the system is precipitation. However, it is assumed that groundwater flow entering the watershed up slope flows beneath the watershed, or that water entering the watershed, plus infiltration within the watershed, are in a steady state with groundwater outflow. This leaves the sinks for water as evapotranspiration, surface outflow, and infiltration. Precipitation, evapotranspiration and surface outflow are estimated in this study, and infiltration is calculated by difference (Table 2).

The Garden Basin watershed experiences winds from the WSW on the east-facing slope of the Thousand Lake Anticline (Fig. 1.14). The flow of air over this ridge to the east (Fig. 1.1) creates a rain shadow, which can be seen as the decrease in the precipitation interpolation of Figure 1.17.

This study uses hybrid precipitation calculated from interpolation of nearby weather stations and PRISM averages with data from the period 2014-2018. The results from the Maxey-Eakin method (Avon et al., 1994) are about 10% higher, which may be due to the decreased precipitation caused by the rain shadow. Alternately, the weather station measured the lowest precipitation due to the loss of water due to evaporation and/or sublimation from snow in the

bucket. The hybrid value of 380 mm/yr. from PRISM and MATLAB interpolation was used, while the weather station and Maxey-Eakin methods are believed to be lower and upper bounds respectively.

When this value of precipitation is compared to the 324 mm/yr. of evapotranspiration estimated for an unmodified watershed, about 85% of water is removed by evapotranspiration. The ratio of ET/P is similar to other publications focused on pinyon-juniper forests with values of between 90% and 100% (Lane and Barnes, 1987). The 15% of water unexplained by evapotranspiration is balanced by surface outflow and infiltration. The value of spillage and seepage outflow is equal to 4% of precipitation, leaving infiltration as the remaining 11% (Table 2). The Maxey-Eakin matches this value quite well, suggesting 15% infiltration (Avon et al, 1994) for this precipitation rate. Further information regarding the calculation of flow vectors within the watershed can be found in the Appendix, including transpiration and specific yield studies.

An analysis of pinyon-juniper forest evapotranspiration fluctuations and relative water table changes show a strong cause and effect relationship. The water table sharply declined just as evapotranspiration rates peaked (Fig. 1.11) and increases when evapotranspiration has dropped. This shows the relationship between evapotranspiration and piezometer measurements, like quasi-sinusoidal trends out of sync, with evapotranspiration determining water levels.

During the pinyon juniper's dormancy period, when soil temperatures are <4.4C, water levels increase rapidly (Fig. 1.13). Miller et al. (2005) suggests that pinyon junipers begin their winter dormancy at this soil temperature, suggesting that water levels are tied to pinyon-juniper uptake. There seems to be about 2 month delay from the time that temperatures reach 4.4°C and when water levels increase. The water consumption calculations predict that about 12.6 cm of

recharge could satisfy the pinyon-juniper forest and bring water levels from the fall slump in piezometer data to the ground surface. The estimates for tree consumption of ~150-300 mm/yr likely favor the lower range due to the colder temperatures experienced from September to November. The water level increase indicated from specific yield (232 mm/yr) is within the bounds of transpiration values (156-313 mm/yr), providing a strong argument that the pinyon-juniper forest evapotranspiration is the main driver of water levels, and thus, the driving variable of pond vs. wetland (drier) conditions.

Precipitation Needed for a Pond State

Piezometer and precipitation data were used to estimate the amount of precipitation necessary to cause the current GBC fen to remain a pond state all year long. The piezometers measured plateaus in water levels when the fen was continuously spilling, and the survey of the area helped to determine the amount of time that GBC fen held any amount of water. Based on four years of data, a graph of days of standing water vs. precipitation (Fig. 1.19) produced a linear trend ($y=1.7667$, $R^2=0.0.2124$). Although this correlation with a very small sample size is not significant according to the student T-distribution test, it is currently the only data available for GBC fen. The plot was forced by the logic that in the absence of precipitation there could never be standing water. Extrapolated to 365 days, 644 mm/yr. of precipitation (Fig. 1.19) are required to produce perennial standing water in the GBC fen. This suggests that the watershed would need to experience an extra ~260 mm/yr. of precipitation to change GBC fen to a pond based on PRISM 30 yr. Averages (PRISM, 2019).

Other drivers of pond-formation, namely the North American monsoon (NAM), were explored that may require less of a precipitation increase. The North American monsoon (NAM) drives an increase in late summer storms and can reach into parts of southern Utah (Grantz et al.,

2007). Evidence of NAM in central Utah has been suggested by pollen data (Shurtliff et al. 2017) and a northward displacement of tropical Pacific cyclones (Barron et al., 2012). Its current effect is seen in the monthly precipitation values of neighboring Arizona found using PRISM (PRISM, 2019). There is a peak in precipitation peaking in August due to the NAM's affect in Central Arizona (Adams, 1997). If the area influenced by NAM reached into the GBC fen area in the past, it may have drastically changed the ecology and hydrologic patterns of the watershed in question. Both methods of (1) estimating tree consumption and (2) calculating specific yield suggest that ~150-300 mm/yr of added precipitation during late-summer may support a pond environment.

CONCLUSIONS

The small watershed in question lies on top of the Windy Ridge mega-landslide that has created a hummocky surface and a complex subsurface of slip surfaces and a mixture of multiple stratigraphic layers.

Extrapolation of spill durations suggest ~260 mm/yr, whereas PJ water demand and specific yield study suggest between 150 to 300 mm/yr monsoon to maintain standing water conditions. The addition of monsoonal precipitation during late summer may better prevent the decline in water levels during autumn (Fig. 1.10; Fig. 1.11), when pinyon-junipers are actively removing groundwater. This is echoed by Shurtliff et al. (2017), who saw high NAM values when GBC was wetter.

The use of this water balance study to determine pond conditions does not have the lag time of the pollen record. Pollen can record precipitation changes, but it takes 50-100 years for the vegetation assemblage to adjust (Shurtliff et al., 2017).

GBC wetland's water balance is dominated by the evapotranspiration of the pinyon-juniper

forest, as water levels decrease during periods of high evapotranspiration (Fig. 1.11). Furthermore, water levels begin to peak when pinyon-junipers are dormant during the coldest months (Fig. 1.13).

CHAPTER 2: CORE ANALYSIS

INTRODUCTION

This chapter describes background studies conducted in support of Hudson et al. (2019). The Windy Ridge mega-landslide, on which GBC watershed resides (Fig. 1.1), covers an area of almost 30 km^2 (Nelson 1989). The slide created hummocky topography with internally drained swales that became sediment traps (Shurtliff et al, 2017). These traps can be seen as fens, ponds, and grassy areas within the lobes of the mega-landslide, which last slipped ~12,600 years BP (Shurtliff et al., 2017). Since the event, organic-rich sediment containing climatic information has been deposited in the fen. For further discussion on the hydrogeological setting and landslide history, please refer to Nelson (1989), Shurliff et al. (2017), and/or Hudson et al. (2019).

GBC fen contains a large patch of cattails in its center, which stores water for the longest amount of time, while grasses grow during the decline in water levels in fall (Fig. 2.1). Cattail species thrive in water of less than 0.45m in depth (Ochterski, 2003). The elevation survey referenced in Chapter 1 (Fig. 1.6) measures the maximum water level in GBC at 0.31m.

A ~3.5m core was extracted near the depocenter of the fen (Fig. 2.1) and analyzed using environmental scanning electron microscopy (ESEM), visual characterization (color and texture), and high resolution (every 3 cm) pyrolysis analysis. These data was then compared to pollen and diatom counts conducted on a previous core of the fen (Shurtliff et al., 2017). Hydrogen indices (HI) were measured for this study through RockEval pyrolysis, and this dataset serves as a proxy for organic matter type and abundance through the cored history of the fen (Hudson et al., 2019).

Previous studies in the area suggest that GBC fen has experienced swings from wetland with no standing water to perennial pond and vice versa (Shurtliff et al., 2017; Hudson et al., 2018), likely driven by changes in precipitation. This chapter explores two drivers for the changes in

GBC fen over the past ~12,500 years: (1) changes in precipitation and (2) physical and basin fill processes. Increases in either annual precipitation or monsoon-derived summer precipitation, as discussed in chapter 1, could lead to a higher water table, and thus more pond-like conditions. Alternately, the basin was ~6m deeper (Shurtliff et al., 2017) in the past, which may have resulted in a potentiometric surface that was much higher relative to the top of the fen sediment, forming pond-like conditions without a change in precipitation. This assumes the spill point elevation has not been changed in the last 12,500 years, which seems unlikely.

This study attempts to qualitatively further understand the nature of the climate record of GBC fen, within the context of the water budget of Chapter 1. Physical alterations from the surface outflow history are also explored.

METHODS

Core

A location was chosen at a low point within GBC fen <3m from the location of a previously collected core (Fig. 2.2). This new core (GBC2) was collected following the methods of Shurtliff et al. (2017).

The core was split lengthwise, placed in vacuum-sealed bags, and refrigerated at ~5°C to retain moisture and retard microbial growth. One core half was used for analysis while the second half was archived for future studies. Photographs of each core sleeve were taken using a 14-megapixel camera and descriptions were made using the USGS Rock-Color Chart. GBC1 was then stratigraphically correlated to GBC2.

Age Determination: Five subsamples were taken from GBC2 at specific textural and color transitions. These subsamples were acid-base-acid washed (Olsson, 1986) and rotting stems and seeds were extracted by using a microscope and fine tweezers. The material was combusted in a

tube furnace at 400°C under an O^2 stream to produce carbon dioxide, and the gas was sent to the University of Georgia Center for Applied Isotope Studies Accelerator Mass-Spectrometer for age determination. Radiocarbon ages were then converted to calibrated ages using Calib 7.1 software (Stuiver et al., 2019). The age-depth profile of this core (GBC2) was plotted with that of the previous core (Fig. 2.3).

Environmental Scanning Electron Microscope (ESEM) Imaging: ESEM images were taken at three points throughout the core (Locations seen in Fig. 2.4). Points were chosen from areas with distinct visual or textural changes in sediment: (1) a segment of especially dark peat, (2) a sharp transition from dull orange to black, and (3) in olive black sediment just below cyclical layers of green, black, and tan (Figure 2.4). The sediment was attached to specimen stubs using double sided carbon tape. The sample was then imaged using the ESEM XL30 FEI instrument at the Brigham Young University Microscopy Lab.

Pyrolysis: Pyrolysis was conducted on a sample of material centered every 3 cm. Each subsample was freeze-dried, ground using mortar and pestle, sieved through 40-mesh, and analyzed using the Wildcat Technologies HAWK Resource Workstation. The workstation dually exposes the samples to increasing temperatures and records the decomposition of hydrocarbons. This process is conducted once with a hydrogen carrier gas to calculate hydrogen index (HI) and total organic carbon TOC (among other indices), then again with a helium carrier gas to find oxygen index (OI). A lower starting temperature (180°C) with a heating rate of 30 °C/min suggested by Baudin et al. (2015) for more modern sediment was used during the first stage of combustion up to 650°C. The second stage was longer and hotter with 300 to 850 °C at a rate of 25 °C min/1. These results are published in Hudson et al. (2019), which provides further detail describing the pyrolysis process.

RockEval Climate Proxy

Hydrogen Index: The modified Van Krevelen diagram (Figure 2.5) shows the endmembers from terrestrial organic matter (wood and coal of type 3) and lacustrine algal organic matter (algae and bacteria of Type 1 (Hudson et al., 2019)), as identified primarily by the Hydrogen Index (HI) of the samples. These two endmembers can be used as a scale from pond conditions dominated by algae (high HI) and more terrestrial conditions dominated by vascular plants (low HI). These endpoints of higher and lower effective moisture provide the foundation for the use of HI as a climate proxy. More details about the various kerogen types are found in Hudson et al. (2019) as well as others that pioneered the use more broadly (Van Krevelen, 1950; Peters, 1986; Espitalié et al., 1977). Further analysis of past precipitation was examined from HI values conducive to a pond environment as previously published (Talbot and Livingstone, 1989: Bonnefille, 1986).

Total Organic Carbon: TOC has been used to reconstruct precipitation regimes in lake sediment (Xu et al., 2006) due to its direct correlation to moisture levels. In this study, TOC is examined as a way in which to indicate the past precipitation regimes of the watershed.

Pollen Counts: Pollen counts sagebrush, amaranth, and ragweed are tabulated by Shurtliff et al. (2014) on GBC-2 core are used as proxy for monsoonal and annual precipitation during the past. Sagebrush to amaranth (SA) is an indicator of annual effective precipitation (Louderback & Rhode 2009; Morris et al. 2013), while Sagebrush vs. Ragweed (SR) is indicative of the North American monsoon (Morris et al. 2013).

Diatoms: Shurtliff et al. (2017) performed an analysis of diatoms in GBC1 at 6cm intervals, creating a diatom history for GBC fen. The diatom remains were separated into wet and dry endmember categories from cat.1 (requiring standing water) and cat. 5 (thriving in periodically wet soil; van Dam et al., 1994). The abundances of these diatoms can differentiate between

standing water conditions (likely with more precipitation) and drier solely wetland conditions.

Sediment Color and Texture: Changes in the color of sediment of can describe changes in environmental conditions (Fitcher, 2015). Similarly, ESEM images give insight to the organisms and minerals that grew and was deposited in GBC fen.

RESULTS

Core

Radiocarbon Ages: Using the Calib 7.1 program (Stuiver et al., 2019; Table 3), calibrated years before present were calculated for material extracted from 5 points within the core (Table 3). The age depth model (Fig. 2.1) was used to convert age from depth estimates by interpolation, assuming a zero age for the top of the core.

Core Description: The core was analyzed by color, grain size, and texture (Fig. 2.2), and split into four time periods:

Younger Dryas (11.8 -11.7 cal ka BP) and Pleistocene to Holocene (P-H) Transition (11.7-9 cal ka BP): This period of the core is dominated by thick, black peat. Although there are slight variations in the color, such as some greyish yellow and dusky brown later in the sequence (~190 cm or 10 ka BP).

One ESEM sample was taken at 230 cm (~10.7ka BP) from this sequence. This sample contained about 90% woody material (some >5mm) including microfossils such as diatom fragments (Figure 2.6). Organic material in these analyses dominate with very little inorganic sediment input.

Early Holocene (9-6 cal ka BP): Visual inspection of this section suggests a transition into more brownish greys and greyish blacks. This sequence contains finer sediment, without the

same abundance of wood fragments seen in the Pleistocene to Holocene transition.

An ESEM image was obtained at 148 cm (9.2ka BP) from the top of the core where sediment was transitioning from dusky brown with large wood fragments to Grayish Yellow with smaller plant fragments. This sample contained wood fragments ornamented with two kinds of brighter grains, which suggests elements of greater atomic mass in the back-scatter images. Figure 2.7 shows bright, flat grains that contain high amounts of aluminum, suggestive of clay. SEM imaging found specks of brighter euhedral pyrite crystals, as confirmed from their high iron and sulfur content (Fig. 2.7).

Middle Holocene (6-3 cal ka BP): This sequence exhibits a change of color toward olive green in the core sediment. The upper half of the sequence is dominated by pale yellowish brown, pale brown, and olive black. The ESEM sample from this sequence was located at 68 cm (3.9ka BP) below the surface at the base of laminations (Fig. 2.4) that were oscillating from olive black to pale brown. The lightest color in this sequence was analyzed in ESEM and found to contain almost exclusively diatom fragments (Fig 2.8). Intercalated are thin (<5mm) dark layers that are similar to the sediment seen in the Early Holocene.

Late Holocene (3 cal ka BP to Present Day): The latest time period corresponds to dusky yellowish browns that are interrupted by lighter, pale browns. However, the upper portion of the sequence turns from dusky browns to greys to blacks. The upper 60% of this sequence is dominated by a mat of small rootlets, which probably result from modern cattails.

The general color transitions of GBC2 core may give insight to a generalized history of the watershed. There is overwhelming black coloration below ~150 cm, which transitions to more greys and dark browns from 150 to ~100cm. This then leads into deep greens from ~100 to 50

cm. Finally, rich browns dominate the upper 50 cm with a black cap at the top (Fig. 2.4).

Trend in Climate Proxies: Each of the climate proxies correlated to higher precipitation values show a pattern similar to the other data sets measured from GBC fen, including pollen, cat. 1 diatom, HI, and TOC (Fig. 2.9). This trend shows higher values with greater frequency and amplitude in the earliest stages of the fen's development, followed by an overall decrease in values and frequency, and ending in an increase in more recent times. HI plotted against TOC correlate with an r-squared value of 0.215, which is significant at $<<0.01$ by the student's t-distribution test assuming 114 data points. Counts of cat. 1 diatoms, which can be used as a proxy for more wet (standing water) environmental conditions (Shurtliff et al., 2017), and therefore show similarities to HI and TOC. For example, higher values in the last ~1.5 ka BP are seen as an increase in cat. 1 diatoms. Subsequently, cat. 5 diatoms (periodically wet soil) increase sharply during the increase of HI, TOC, and cat. 1 diatoms. The years preceding 9 ka BP show highest values in all data sets (except cat. 5 diatoms) with relatively higher variability in the data sets. The trend is seen in precipitation indicated from pollen indices including: (1) maximum values at 10-11 years BP, (2) higher amount of variability after ~9.5 ka BP, and (3) depressed values in the early and middle Holocene times (~9 ka BP to 2 ka BP).

Color variations correlate to TOC. Fig. 2.9 depicts that TOC weight percent of <10% coincide with brownish or greenish sediment, which suggest a drier environment. Furthermore, greys and blacks tend to occur at TOC levels of >10%. This result agrees well with other studies such as Nederbragt et al. (2006) that have found a correlation between TOC levels and sediment color, noting that sediment lightness becomes saturated at higher TOC concentrations >10%.

Sedimentation Rate of GBC1: The age-depth profile from both the GBC1 and GBC2 cores taken within the fen (Fig. 2.3) reveals a relatively high sedimentation rate (~0.15 cm/yr.) from

about 338 to 150 cm depth (~11.3 to 9 ka BP). The slope then shallows to a sedimentation rate of around 0.02 cm/yr., only to rise again at 20 cm to 0.06 cm/yr. The section below 150 cm within GBC2 consists of a sludge of thick peat material and clay, while the area above this mark is relatively lighter with browns, greys, and olive greens (Fig. 2.4). The lighter colored materials correlate with lower sedimentation rates, whereas the darker areas correspond to rapid sedimentation (Fig. 2.9).

DISCUSSION

Changing Sill Altitude

The barrier formed on the east side of the fen is the determining factor in water height in the fen when water input is great enough to spill (Chapter 1). Shurliff et al. (2017) concluded that GBC fen was more pond than fen early (especially from 11.5 to 10 ka), although the diatoms did show a lot of oscillations between wet and dry during this period. Therefore, if the spill point has not moved, it had to be unrealistically dry when the top of the fen sediment was several meters deep to accommodate the dry oscillations. The pollen of wetland species such as *Betulaceae* and *Salicaceae*-Salix are present throughout, suggesting shallow water for the last 12.5 ka (Shurtliff et al., 2014; their Fig. 10). This coincides with the abundance of woody material and fibrous roots (Fig. 2.2; Fig. 2.6) found below 200 cm in GBC2 core. A shallow-water environment seems counterintuitive when considering the fen was originally 6 m deeper than present day, and modern piezometer measurements from 2015 to 2018 never drop more than ~0.7 m below the modern fen surface (Fig. 1.10). In order to sustain shallow water levels throughout the fen's history, the spill point must have changed elevation.

Beavers, like those seen just 3.7 km to the NW (located at 460401E, 4265288N), may have played a dominant role in raising the height of the spill point. If beavers were able to continually

inhabit the fen, they may have created a condition where the spill point elevation increased as the sediment water/sediment air interface also rose. In other words, the distance between the spill point and the base of the fen may have stayed relatively constant. Although beavers have no effect on rainfall, they can progressively allow GBC to be a pond when rainfall was high enough, elevating climate proxies such as HI, TOC, and cat. 1 diatoms. Furthermore, beaver activity is known to cause high sedimentation rates by trapping sediment (USGS, 2018). The Pleistocene to Holocene transition happens to correlate well to each of these characteristics, suggesting that beavers may have inhabited GBC fen at the time.

On Nov. 5, 2019, simple 1D MASW experiments (Park et al., 1999) were conducted on the outflow barrier to the GBC fen, as well as on nearby landslide material. The shear-wave velocity of near-surface material on the landslide was 180 m/s, whereas the outflow barrier was 130 m/s. Overall, the dispersion curves were different as well, indicating that the barrier and landslide are composed of different materials (S. Nelson, written communication, 2019). This may indicate that the barrier represents altered landslide material from beaver in the area.

The GBC watershed is currently grazed by cattle. It is possible that this barrier has been raised by ranchers to provide water for cattle. Assuming the barrier has been raised by human activity from the seepage point elevations .41 to .33 m below rim corresponds to ages in the core of over 1000 yr BP. This predates settlement of the area by almost 750 years, suggesting more natural causes. The organic mud in the fen is nearly impossible to walk in, so the use of hand or power machinery seems improbable given the narrow width of the top of the barrier. Furthermore, there is no evidence of a nearby borrow pit or trench.

Core

The Younger Dryas (11.8 -11.7 cal ka BP) and Pleistocene to Holocene (P-H) Transition

(11.7-9 cal ka BP) exhibit characteristics indicative of higher precipitation and relatively anoxic conditions, likely due to a longer duration of standing-water conditions. The ESEM analysis performed at 190 cm on black silty peat suggested relatively anoxic water (Fig. 2.10). This coincides with an ESEM image (Fig. 2.7) of wood fragments ornamented euhedral pyrite crystals, which suggests reducing conditions and pyrite crystallization (Feick, 2014). Groundwater flowing through ferrous Tertiary volcanic rock (Nelson, 1989) acts as a sink for O_2 and (3) the sulfate content of the Morrison Formation provided a source of sulfate ions for pyrite formation (Cadigan, 1967; Rheubottom, 2006) under reducing conditions.

Other climate proxies for this time suggest a relatively high effective moisture. The dark sediments exhibit elevated levels of TOC and HI during this period (Fig. 2.9) suggesting the relative high algal productivity of a pond environment. The high algae production is consistent with annual and monsoonal precipitation reaching their maxima during this episode. Sedimentation rates also reached their highest levels during this period. Figure 2.9 shows a large peak in cat. 1 diatoms (standing water), which tapers off to reveal a spike in cat. 5 (regularly damp soil). This suggests an abundance of moisture, followed by a drying period coinciding with a decrease in effective precipitation starting in the Early Holocene period described in Shurtliff et al. (2017).

Sediment from the Early Holocene (9-6 cal ka BP) is dominated by lighter colored sediment and correlates to decreasing amounts of TOC (Fig. 2.9). This decline over the course of ~3 ka, coincides with decreasing HI values, pollen proxies for precipitation, and sedimentation rates. The decreased precipitation reflected in the pollen record may have decreased the duration of standing water in GBC fen, thus decreasing algal production. Additionally, as basin fill raised the surface of GBC fen in relation to the water table and the spill point, water levels within the fen

would have decreased. Each of these factors may describe a period of decreased effective precipitation, likely caused by increasing temperatures, seen in a summary of climate proxies (of the western United States) compiled by Shurtliff et al. (2017; their Fig. 10).

ESEM images taken for the Middle Holocene Epoch (6-3 cal ka BP) depict skeletal diatoms and little else. In the section spanning 50cm to 80cm (Fig. 2.2), cyclical patterns of brown and green may indicate a transition from deeper (more anoxic) pond to wetland envrionment. A decrease in the duration of standing water likely brought the surface of the fen in contact with the atmosphere for longer, providing an aerobic environment. Additionally, the dominant brown color with high root concentrations in the Late Holocene may be an indication of vascular plants taking advantage of lower water levels.

Figure 2.9 shows the lowest values of HI and TOC occurring in the Middle Holocene time. The production of organic material (both algal and terrestrial) may have been detrimentally affected by relatively low precipitation, as indicated by low pollen ratios. Note how the overall negative slope of TOC values at the beginning of this time period become shallower as precipitation, while still relatively low during the Early and Middle Holocene time, increases gradually during this episode (Fig. 2.9). The increase in precipitation likely caused a slight increase in cat. 1 diatoms (wetter) as cat. 5 diatoms decreased. HI values seem to oscillate between the lowest values (~200 mgHC/gTOC) and ~300 mgHC/gTOC. Hudson et al. (2019) suggested that high biogenic silica content from high amounts of freshwater diatoms may also suppress HI values. Thus, the low HI values may be caused by dominance of diatoms vs. green/blue-green algae, suggesting the continuance of an aquatic environment.

The lower values of HI may also be due to a peak in vascular plants preferring shallow water like cattails and grasses that currently dominate GBC fen. These plants may not have been

able to grow in previously relatively anoxic or deep-water conditions, but a decreased basin depth or decrease in precipitation could have caused them to flourish in a shallower environment. If this is the case, not only would there be higher amount of terrestrial organic matter, but the decrease in sunlight reaching the water may prevent algae from performing photosynthesis.

The darker material of the Late Holocene (3 cal ka BP to Present Day) sequence of the core, with its high values of TOC, HI, and pollen ratios indicates an increase in water depth with increased precipitation. This correlates to a mid- to late-Holocene episode of higher effective precipitation greater than or equal to that of the present climate documented seen in other proxies of the western US (Shurtliff et al., 2017). The midpoint of this episode occurs at ~1.9 ka BP, and corresponds to a large peak in water-loving diatoms (cat. 1) and nearly nonexistent cat. 5 diatoms (Fig. 2.9).

The core is topped by a 5cm layer of black sediment intercalated between dark-grey strata where TOC levels double, HI values increase by 22% and sedimentation rates increase sharply. The increase in TOC, HI, and sedimentation rate would point to an increase in effective moisture. However, pollen ratios suggest a sharp decrease in monsoonal input (SR) and a stabilization of annual precipitation (SA; Fig. 2.9). Anthropogenic alteration to the watershed, mainly through the clearing of pinyon-juniper forest, may have drastically decreased the evapotranspiration potential of the watershed. Rangelands evapotranspire at least 28% less than pinyon-juniper forest, thus the lack of forest would act as an increase in moisture input to the GBC fen. This coincides with the increase in TOC, HI, and sedimentation rate, while still accounting for the lack of increase in precipitation exhibited by the pollen record. One must also consider that the introduction of cattle into ephemeral wetlands has been known to extend periods of standing water (Pyke, 2005). It is possible that this process may have aided the increase the evidence of effective moisture at the

cap.

Constant Sill Altitude

Although the a unvarying sill altitude is considered very unlikely from the pollen record, many of the characteristics contained in GBC2 core also correlate to a fen with constant sill altitude. This scenario assumes that the Windy Ridge landslide created a GBC basin 6 m in depth with a spill point at its current elevation at 12,500 yr BP, the age of the oldest sediment in the wetland (Shurtliff et al., 2017). Deeper portions of the GBC2 core consist of sediment dominated by high amounts of organic material with small amounts of inorganic clay and silt particles. This is consistent with a relatively deep/anoxic pond environment created from a spill point high in elevation. A change from relatively deep-water to a shallow-water/wetland environment as the basin filled with sediment is consistent with the overall color transitions of the GBC2 core (Fig. 2.10). The change from black to grey to green to brown may indicate increasing oxygen levels or water circulation (Fig. 2.10) and be an identifier of the past environment, changing from more deep/anoxic water to shallower/aerobic conditions.

Quantifying Historical Precipitation

Many of the proxies discussed could be used as environmental indicators of pond (wetter) and wetland (drier) environments. Hydrogen Index is one of the indicators emphasized and may give more insight to the precipitation of specific periods in the fen's past. Two possibilities were explored: (1) Talbot and Livingstone (1989) suggest algae/bacteria [or pond environment] create a signature > 750 HCmg/TOCg and suggest wood and coal [or wetland environment] at <200 HCmg/TOCg and (2) Bonnefille (1986) gives bounds of between >400 HCmg/TOCg and <100 HCmg/TOCg. The latter was preferred, because Talbot and Livingstone's values would preclude a pond state in the GBC fen record, which is clearly contradicted by the diatom record.

Figure 2.11 seems to mirror what has been shown in other publications (Shurtliff et al, 2017 and Hudson et al., 2019), with pond conditions during the early Holocene. This was then followed by a drying period during the middle Holocene that rebounded in the most recent past. During pond periods, there was likely >644 mm/yr of precipitation or 150-300 mm/yr of additional monsoonal input (Chapter 1), whereas wetland states were below these values.

Two pollen groups, *Pinus* and *Pinus*-hap, show that at around 9 ka years BP there may have been a change in the composition of the PJ forest (Shurtliff et al., 2017). The amount of spruce tree (*Picea*) count decreased drastically and the PJ (as suggested by *Pinus*-hap) count increased significantly (Fig. 2.12). This indicates that the tree line lowered to the point where a spruce trees were in much closer proximity. Spruce-fir forest, which is the fourth most common forest in Utah (McAvoy et al., 2012), may have been encroaching on or overtaken the watershed. The spruce-fir type forests of Utah contain mainly Engelmann spruce (*Picea Engelmannii*) with douglas and subalpine fir (McAvoy et al., 2012). Engelmann spruce tend to thrive in areas with higher precipitation on the order of 600 to 1400 mm/yr. in their Utah ranges (Alexander, 1984). PJ forests, like the one seen on Garden Basin watershed, thrive in precipitation of between 250 and 500 mm/yr (CSFS, 2009; Wiese, 2000). Figure 2.12 may suggest a change in precipitation from between 600-1400 mm/yr to 250-500 mm/yr, although it may just indicate the transgression of spruce forest. These two environments tend to bound the 644 mm/yr calculated for pond/wetland conditions.

CONCLUSIONS

This study shows great similarities in the trends of HI, TOC, pollen, diatom, sedimentation rates, and sediment color as proxies for effective moisture over time. It seems that there are two main drivers for environmental change within the GBC fen: Core analyses point to a long period

of high effective moisture (12-9 ka BP) after the Windy Ridge landslide last moved, followed by a freshwater-dominated environment punctuated by dry episodes. Subsequently, precipitation decrease from 9-3 ka BP led to a dominance by wetland rather than standing water. Late Holocene sediments suggest a return to greater precipitation from 3 ka BP to present.

This pattern of climate variability is consistent with Shurtliff et al. (2017), who reviewed a number of proxy records for the western US (Fig. 2.13). The midpoint of the Mid-Holocene low precipitation event occurs during drop in precipitation at ~7 ka BP and the midpoint of the Late Holocene high precipitation event occurs during a period of rebound in precipitation (Fig. 2.9 & 2.13).

A preponderance of the evidence suggests that the elevation of the outlet of the GBC fen has evolved with time as the basin has filled with sediment, likely from beaver activity. The water budget in Chapter 1 suggests that in its current configuration that precipitation increases of 150 to 300 mm/yr., depending on whether it is annual or seasonal (i.e., NAM), may produce perennial standing water in what is typically wet ground for >50% of the year. Assuming that the average difference elevation of the spill point and fen surface have remained constant, similar fluctuations in climate may have driven the conversion of fen to pond (and vice versa) in the past.

REFERENCES

CHAPTER 1

Adams, David & Comrie, Andrew. (1997). *The North American Monsoon*. Bulletin of the American Meteorological Society. 78. 2197-2213. 10.1175/1520-0477(1997)078<2197:TNAM>2.0.CO;2.

Allen, R.G., L.S. Pereira, D. Raes, D., and M. Smith. 1998. *Crop evapotranspiration, guidelines for computing crop water requirements*. FAO Irrig. and Drain. Paper 56, Food and Agric. Orgn. of the United Nations, Rome, Italy. 300 pp.

Avon, L. and Durbin, T. J. (1994), *Evaluation Of The Maxey-Eakin Method For Estimating Recharge To Ground-Water Basins In Nevada1*. Jawra Journal of the American Water Resources Association, 30: 99-111. doi:10.1111/j.1752-1688.1994.tb03277.x

Barron, J.A., Metcalfe, S.E., Addison, J.A., 2012. *Response of the North American monsoon to regional chances in ocean surface temperature*. Paleoceanography, v. 27. http://dx.doi.org/10.1029/2011PA002235.

Bear, J. (1972). Dynamics of Fluids in Porous Media. Dover Publications. ISBN 0-486-65675-6

Bedell, T.E., 1993, *Western juniper: its impact and management in Oregon rangelands: Corvallis*, Oregon State University Extension Service.

Cook, Benjamin, Ault, Toby and Smerdon, Jason, *Unprecedented 21st century drought risk in the American Southwest and Central Plains*, Science Advances, Feb. 12, 2015, https://tinyurl.com/jqk3ujw.

De Rocher, T.R, Tausch, R.J, *Predicting potential transpiration of singleleaf pinyon: an adaptation of the potometer method*: Forest Ecology and Management, Volume 63, Issues 2–3, 1994, Pages 169-180, ISSN 0378-1127, https://doi.org/10.1016/0378-1127(94)90109-0.

Doorenbos, J. and Pruitt, W. O., 1977. *Crop water requirements*. Irrigation and Drainage Paper No. 24, (rev.) FAO, Rome, Italy. Pg. 144

Google Earth, 2015, Central Utah. 38.513385330°, -111.422499905°, Eye alt 123.23 meters. http://www.earth.google.com. Accessed 10/24/2019

Goulden, M. L., R. G. Anderson, R. C. Bales, A. E. Kelly, M. Meadows, and G. C. Winston, 2012. *Evapotranspiration along an elevation gradient in California's Sierra Nevada*, J. Geophys. Res., 117, G03028, doi:10.1029/2012JG002027.

Grantz, K., B. Rajagopalan, M. Clark, and E. Zagona, 2007. *Seasonal Shifts in the North American Monsoon. J. Climate,* **20**, 1923–1935, https://doi.org/10.1175/JCLI4091.1

Healy, R.W., 2007, *Water budgets: foundations for effective water-resources and environmental management: Reston, VA, U.S.* Geological Survey. https://pubs.usgs.gov/circ/2007/1308/ Accessed 11/17.

HOBO, *Barometric Compensation Method: Barometric Compensation Method | Onset Data Loggers*, https://www.onsetcomp.com/support/tech-note/barometric-compensation-method (accessed September 2019).

Hudson, S.M., Hillam, S.A., Barker, J., Nelson, S.T., and Rey, K.A., 2019, *Pyrolysis of modern wetland sediment: extracting climate records from fens in the Uinta Mountains and Fish Lake Plateau, Utah, USA*: Boreas, doi: 10.1111/bor.12378.

Lane, L. J.; Barnes, F. J. 1987. *Water balance calculations in southwestern woodlands*. Everett, R. L., comp. Proceedings— pinyon-juniper conference. Gen. Tech. Rep. INT-215. Ogden, UT: U.S. Department of Agriculture, Forest Service, Intermountain Research Station: 480-488.

Maxey, G.B. and Eakin, T.E., 1949, *Groundwater in the White River Valley, White Pine, Nye, and Lincoln counties, Nevada*. Water Resources Bulletin No. 8, State of Nevada, Office of the State Engineer.

Miller, R.F., Bates, J.D., Svejcar, T.J., Pierson, F.B., and Eddleman, L.E., 2005, *Biology, Ecology, And Management Of Western Juniper*: Technical Bulletin, Agricultural Experiment Station, Oregon State University , v. 152, https://catalog.extension.oregonstate.edu/sites/catalog/files/project/pdf/tb152.pdf.

Morris, D.A. and A.I. Johnson, 1967. *Summary of hydrologic and physical properties of rock and soil materials as analyzed by the Hydrologic Laboratory of the U.S. Geological Survey*, U.S. Geological Survey Water-Supply Paper 1839-D, 42p.

NASA, 2016, *Index of /archive/geotiff/MOD_NDVI_M*, https://neo.sci.gsfc.nasa.gov/archive/geotiff/MOD_NDVI_M/ Accessed 1/26/18

NASA, 2015, *Earth Observatory*, https://tinyurl.com/ydxxgoa4. Accessed 11/16/17

NASA, 2019, *Global Subsets Tool: MODIS/VIIRS Land Products*, https://modis.ornl.gov/cgi-bin/MODIS/global/subset.pl/ Accessed 10/16/19

Nelson, S.T., 1989, *Geologic Map of the Geyser Peak Quadrangle, Wayne and Sevier Counties, Utah*: Utah Geological and Mineral Survey. 114.

Nimmo, J. R., Horowitz, C. and Mitchell, L. (2015*), Discrete-Storm Water-Table Fluctuation Method to Estimate Episodic Recharge*. Groundwater, 53: 282-292. doi:10.1111/gwat.12177

PRISM (PRISM Climate Group), 2019, http://prism.oregonstate.edu/. Accessed 1/19.

Riddell, E. & Everson, Colin & Clulow, Alistair & Mengistu, Michael. (2013). *The hydrological characterisation and water budget of a South African rehabilitated headwater wetland system.* Water S.A. 39. 57-66. 10.4314/wsa.v39i1.8.

Shurtliff, Ryan Andros, 2014, *Wetlands on the Thousand Lake Mountain Mega-Landslide as Paleoclimate Proxies*. Theses and Dissertations. 4134. https://scholarsarchive.byu.edu/etd/4134

Shurtliff, R.A., Nelson, S.T., Mcbride, J.H., Rey, K.A., Tucker, J.C., Godwin, S.B., and Tingey, D.G., 2017, *A 13 000 year multi-proxy climate record from central Utah (western USA), emphasizing conditions leading to large mass movements*: Boreas, v. 46, p. 308–324, doi: 10.1111/bor.12213.

USGS, 2018, http://earthexplorer.usgs.gov/. Accessed 4/5/18

Zhang, M., Singh, H.V., Migliaccio, K.W., and Kisekka, I., 2017, *Evaluating water table response to rainfall events in a shallow aquifer and canal system*: Hydrological Processes, v. 31, p. 3907–3919, doi: 10.1002/hyp.11306.

CHAPTER 2

Baudin,F., Disnar, J. R., Aboussou, A.&Savignac,F. 2015. *Guidelines for Rock Eval analysis of recent marine sediments*. Organic Geochemistry 86, 71–80.

Bonnefille, R., Robert, C., Lezine, A.M., Perinet, G., Delibrias, G., Elenga, C., Herbin, J.P., and Tiercelin, J.J., 1986, *Palaeoenvironment of Lake Abijata, Ethiopia, during the past 2000 years*: Geological Society, London, Special Publications, v. 25, p. 253–265, doi: 10.1144/gsl.sp.1986.025.01.21.

Cadigan, R.A., 1967, *Petrology of the Morrison Formation in the Colorado Plateau region*: Professional Paper, v. 556, doi: 10.3133/pp556.

CSFS (Colorado State Forest Service), 2009, *Piñon–Juniper Woodlands Colorado State Forest Service*, https://csfs.colostate.edu/colorado-forests/forest-types/pinon-juniper-woodlands/ (accessed August 2019).

Espitalié, J., Laporte, J.L., Madec, M., Marquis, F., Leplat, P., Paulet, J. & Boutefeu, A. 1977: *Méthode rapide de caractérisation des roches métres, de leur potential pétrolier et de leur degré d' évolution*. Revue de I'Institut francais du Pétrole 32, 23–42.

Feick, K., 2014, *Pyrite*: Earth Sciences Museum, https://uwaterloo.ca/earthsciences-museum/resources/detailedrocksandmineralsarticle s/pyrite (accessed January 2019).

Fitcher, L.S., 2000, *Color Interpretations from Sedimentary Rocks*: Color in sedimentary rocks, http://csmgeo.csm.jmu.edu/geollab/fichter/sedrx/color.html (accessed August 2018).

Hudson, S.M., Hillam, S.A., Barker, J., Nelson, S.T., and Rey, K.A., 2019, *Pyrolysis of modern wetland sediment: extracting climate records from fens in the Uinta Mountains and Fish Lake Plateau, Utah, USA*: Boreas, doi: 10.1111/bor.12378.

Louderback, L. A. & Rhode, D. E. 2009: *15 000 years of vegetation change in the Bonneville Basin; the Blue Lake pollen record*. Quaternary Science Reviews 28, 308–326.

Macfarlane, W., Wheaton, J., and Jensen, M., 2004, *The Utah Beaver Restoration Assessment Tool: A Decision Support & Planning Tool*: Final Report To Utah Division Of Wildlife Resources, Utah State University.

McAvoy, D., Kuhns, M., and Black, J., 2012, *Utah Forest Types: An Introduction to Utah Forests*: Rural/Conservation Forestry. Utah State University

Morris, J. L., Brunelle, A., Munson, A. S., Spencer, J., Power, M. J. & Starratt, S. 2013: *Holocene vegetation and fire reconstructions from the Aquarius plateau, Utah, USA*. Quaternary International, v. 310, pg. 111–123.

Nederbragt, A.J., Dunbar, R.B., Osborn, A.T., Palmer, A., Thurow, J.W., and Wagner, T., 2006, *Sediment colour analysis from digital images and correlation with sediment composition*: Geological Society, London, Special Publications, v. 267, p. 113–128, doi: 10.1144/gsl.sp.2006.267.01.08.

Nelson, S.T., 1989, *Geologic Map of the Geyser Peak Quadrangle, Wayne and Sevier Counties, Utah*: Utah Geological and Mineral Survey. 114.

Ochterski, J., 2003, *Controlling Cattails*: Cornell Cooperative Extension, http://franklin.cce.cornell.edu/environment/ponds/controlling-cattails (accessed May 2019).

Olsson, I.U., 1986, *Radiometric dating in Berglund, B.E. ed*., Handbook of Holocene Palaeoecology and Palaeohydrology, J. Wiley, New York, p. 273312

Park, C.B., Miller, R.D. and Xia, J., 1999, *Multichannel analysis of surface waves*, Geophysics, 64(3): 800-803.

Peters, K. E. 1986: *Guidelines for evaluating petroleum source rock using programmed pyrolysis*. American Association of Petroleum Geologists Bulletin 70, 318–329.

Pyke, C. R. and Marty, J. (2005), *Cattle Grazing Mediates Climate Change Impacts on Ephemeral Wetlands*. Conservation Biology, 19: 1619-1625. doi:10.1111/j.1523-1739.2005.00233.x

Rheubottom, A., Webber, C.E., Rozier, G., and Bailey, C.M., 2006, *Volcanic stratigraphy of the Fish Lake Plateau, Utah*: Geological Society of America Abstracts with Programs, v. 38, no. 6, p. 32.

Shurtliff, R.A., Nelson, S.T., Mcbride, J.H., Rey, K.A., Tucker, J.C., Godwin, S.B., and Tingey, D.G., 2017, *A 13 000 year multi-proxy climate record from central Utah (western USA), emphasizing conditions leading to large mass movements*: Boreas, v. 46, p. 308–324, doi: 10.1111/bor.12213.

Stuiver, M., Reimer, P.J., and Reimer, R.W., 2019, CALIB 7.1 [WWW program] at http://calib.org, accessed 3/4/2019

Talbot, M. R. & Livingstone, D. A. 1989: *Hydrogen index and carbonisotopes of lacustrine organic matter as lake level indicators*. Palaeo-geography, Palaeoclimatology, Palaeoecology 70,121–137.

USGS, 2018, *Effects of Beaver Dams on Sediment Transport*: https://www.usgs.gov/media/files/5-effects-beaver-dams-sediment-transport (accessed August 2019).

Van Dam, H., Mertens, A. & Sinkeldam, J. 1994: *A coded checklist and ecological indicator values of fresh water diatoms from the Netherlands*. Netherlands Journal of Aquatic

Ecology 28, 117–133.

Van Krevelen, D.W. 1950: *Graphical-statistical method for the study of structure and reaction processes of coal*. Fuel 29, 269–284

Wiese, K., 2000, *Sierra Nevada wildflowers: a field guide to common wildflowers and shrubs of the Sierra Nevada, including Yosemite, Sequoia, and Kings Canyon National Parks*: Helena, Mont, Falcon.

Xu, H., Ai, L., Tan, L., and An, Z., 2006, *Stable isotopes in bulk carbonates and organic matter in recent sediments of Lake Qinghai and their climatic implications*: Chemical Geology, v. 235, p. 262–275, doi: 10.1016/j.chemgeo.2006.07.005.

CHAPTER 1

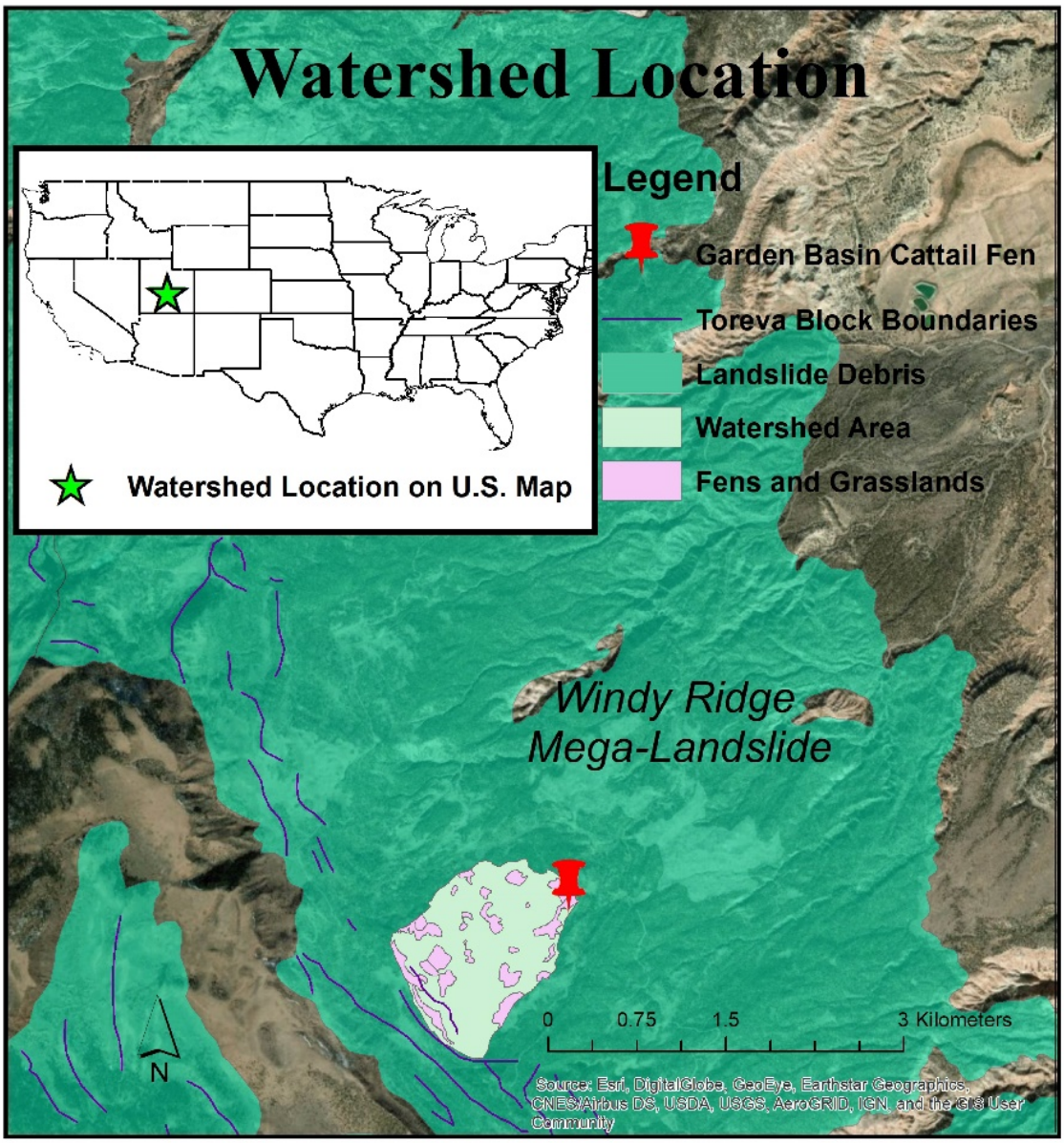

Figure 1.1 Index map depicting the location of the Garden Basin watershed in Central Utah. The map also shows the Windy Ridge landslide, Garden Basin wetlands, and other features discussed in the text.

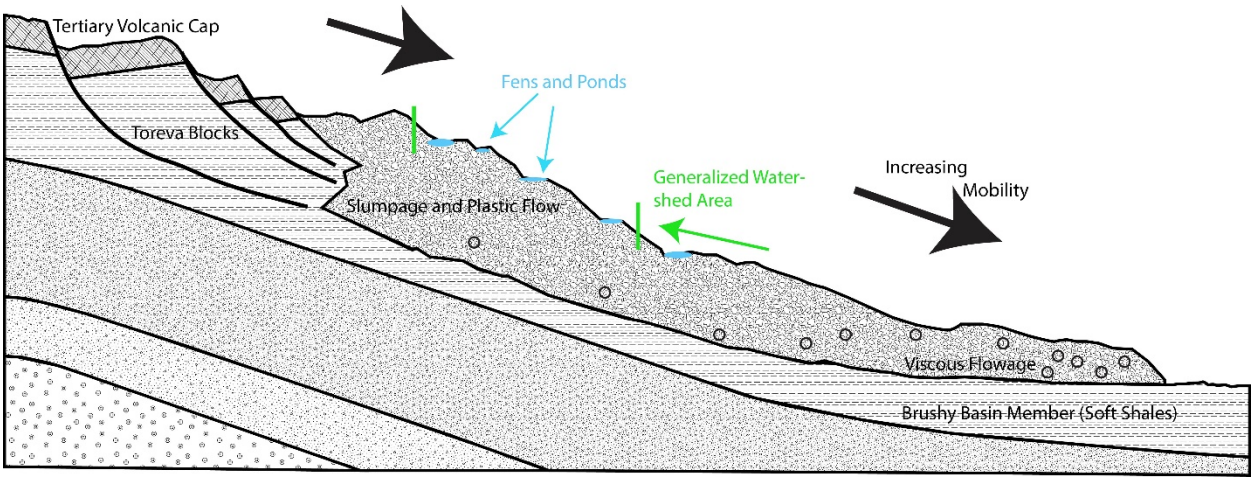

Figure 1.2 This cross section (oriented west to east) shows the basic structure of the Windy Ridge mega-landslide from toreva blocks to the slumpage to the viscus flowage (modified from Nelson, 1989). The watershed in question likely resides in hummocks and swales of the slumpage and plastic flowage portion of the landslide structure. (Shurtliff et al., 2017)

Figure 1.3 This image (apologies for the low resolution) was taken of landslide sediment near the watershed (Shurtliff et al, 2014). This image shows the fine clays of the Brushy Basin member filling the interstices of tertiary volcanic gravel.

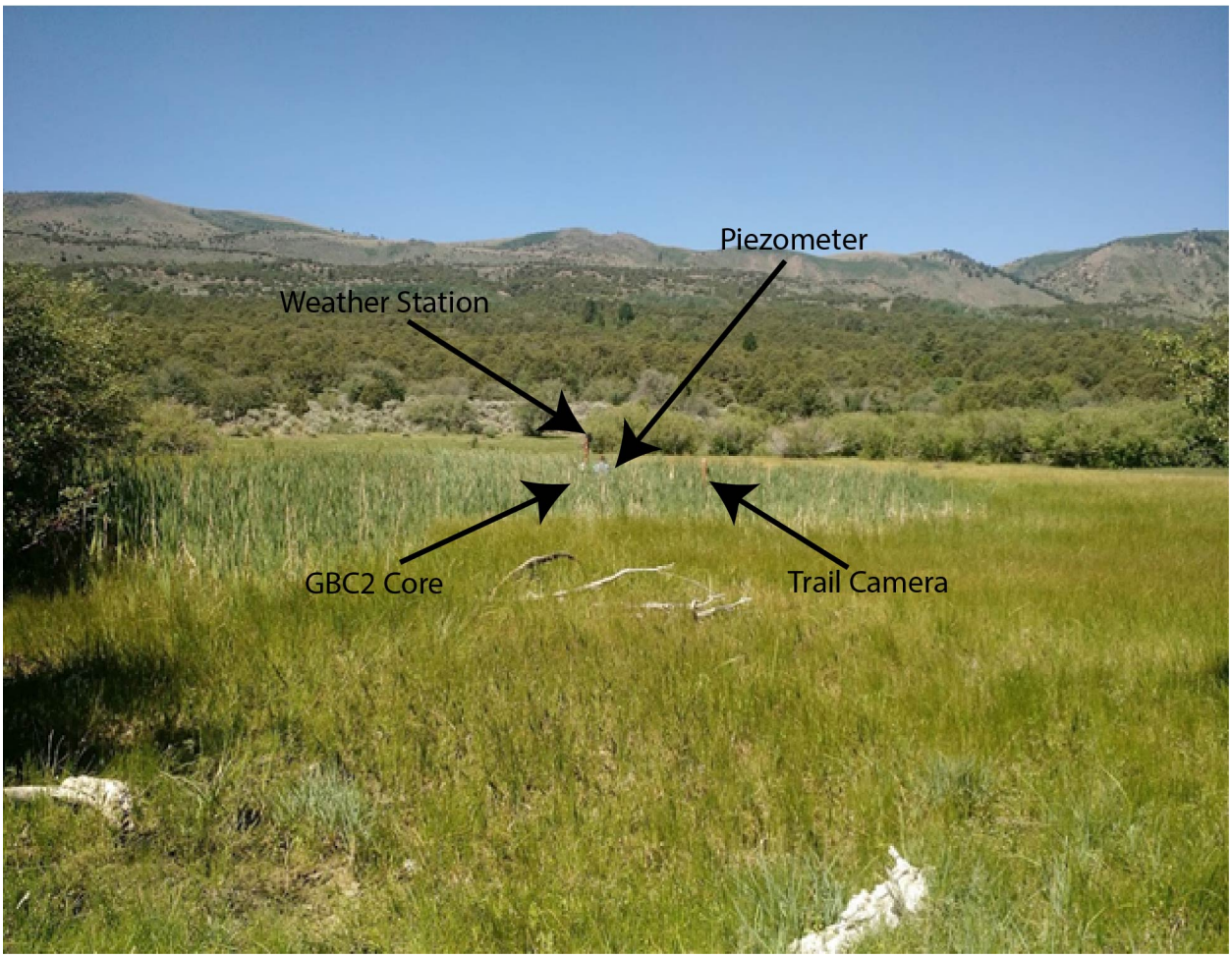

Figure 1.4 This is an image of GBC fen looking west from the spill point. Notice the cattails in the deepest part of the fen, which retains surface water longer than the rest of the body. Long grasses grow around the cattails as water levels decrease.

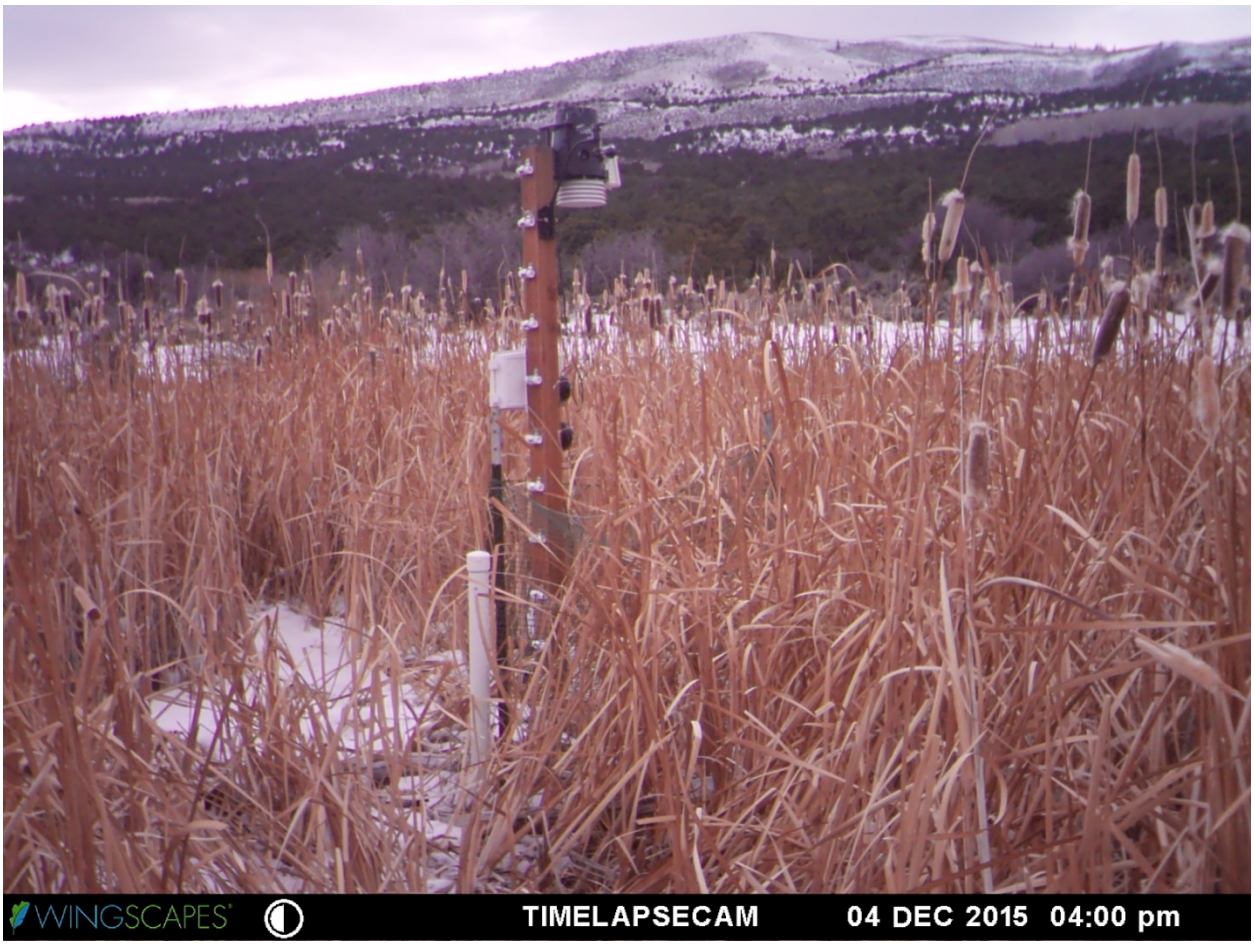

Figure 1.5 Time lapse photo taken in GBC fen from a trail camera positioned just east of the weather station. This photo is indicative of most days during the winter months. Snow falls quite often, but not much of the snow remains around the fen, although snow within the fen itself seems to remain frozen within the fen for longer. The frequent snowfall and melt may be seen as an increase in water level in the piezometer data.

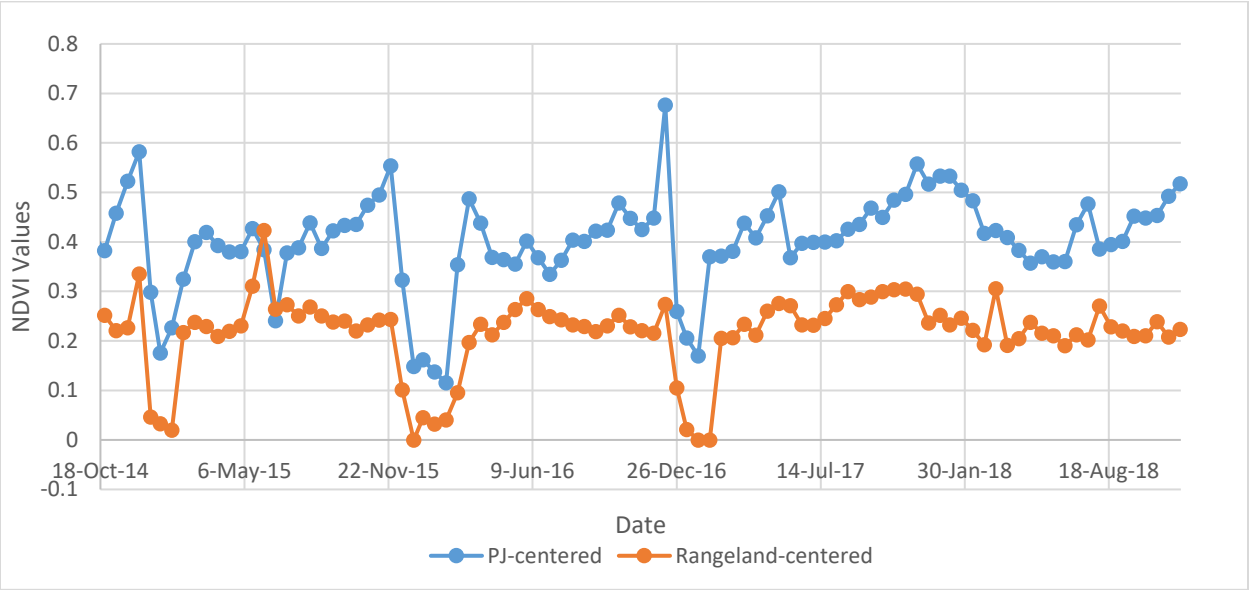

Figure 1.6 The plot shows the discrepancy between NDVI values from PJ forests to grasslands. Each point represents NDVI values (NASA, 2019) taken from a 250 x 250 m pixel centered at PJ forest (blue) or rangeland (orange). Since NDVI is correlated to ET, this plot suggests that deforestation of PJ forest for graze land significantly decreases the amount water taken-up and transpired by vegetation.

Figure 1.7 This image shows the inside of the flow pipe at the east spill point. Notice the hard water buildup along the walls of the pipe, indicated with pink lines. This would suggest a continuous water level in the pipe of 1.5 inches.

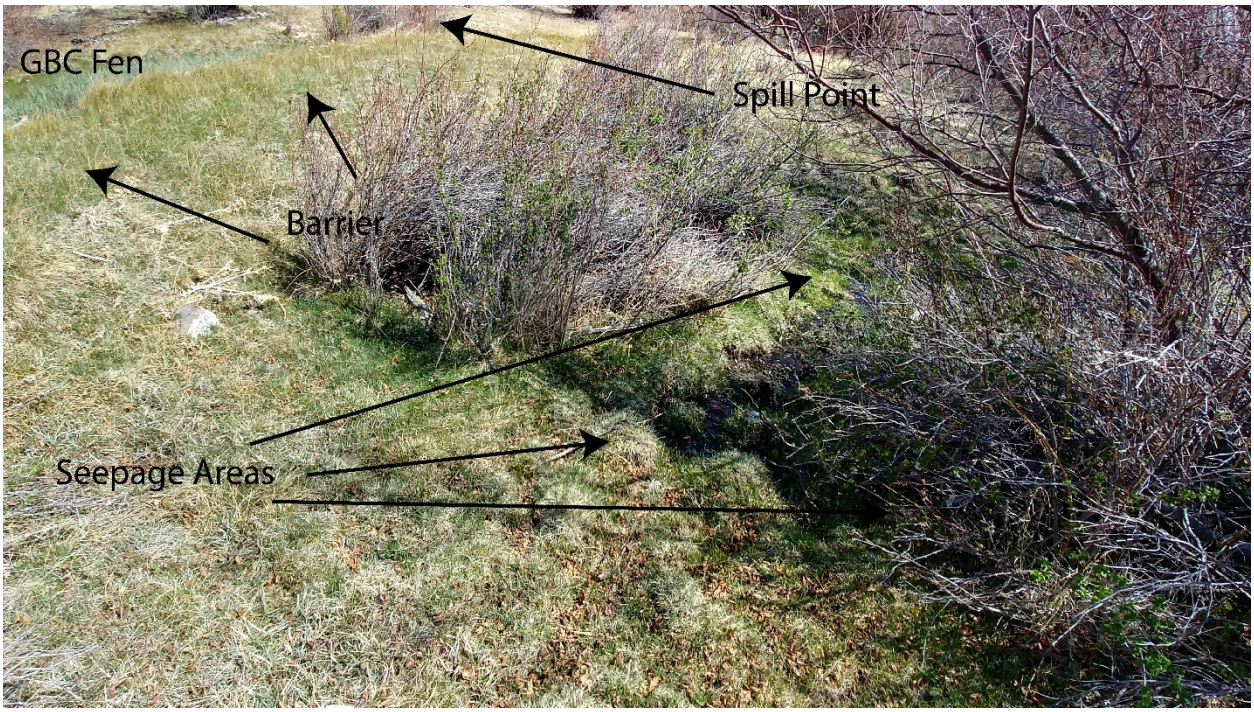

Figure 1.8 Image of the seepage area daylighting to the east of GBC fen. Locations for the barrier and spill point are also indicated.

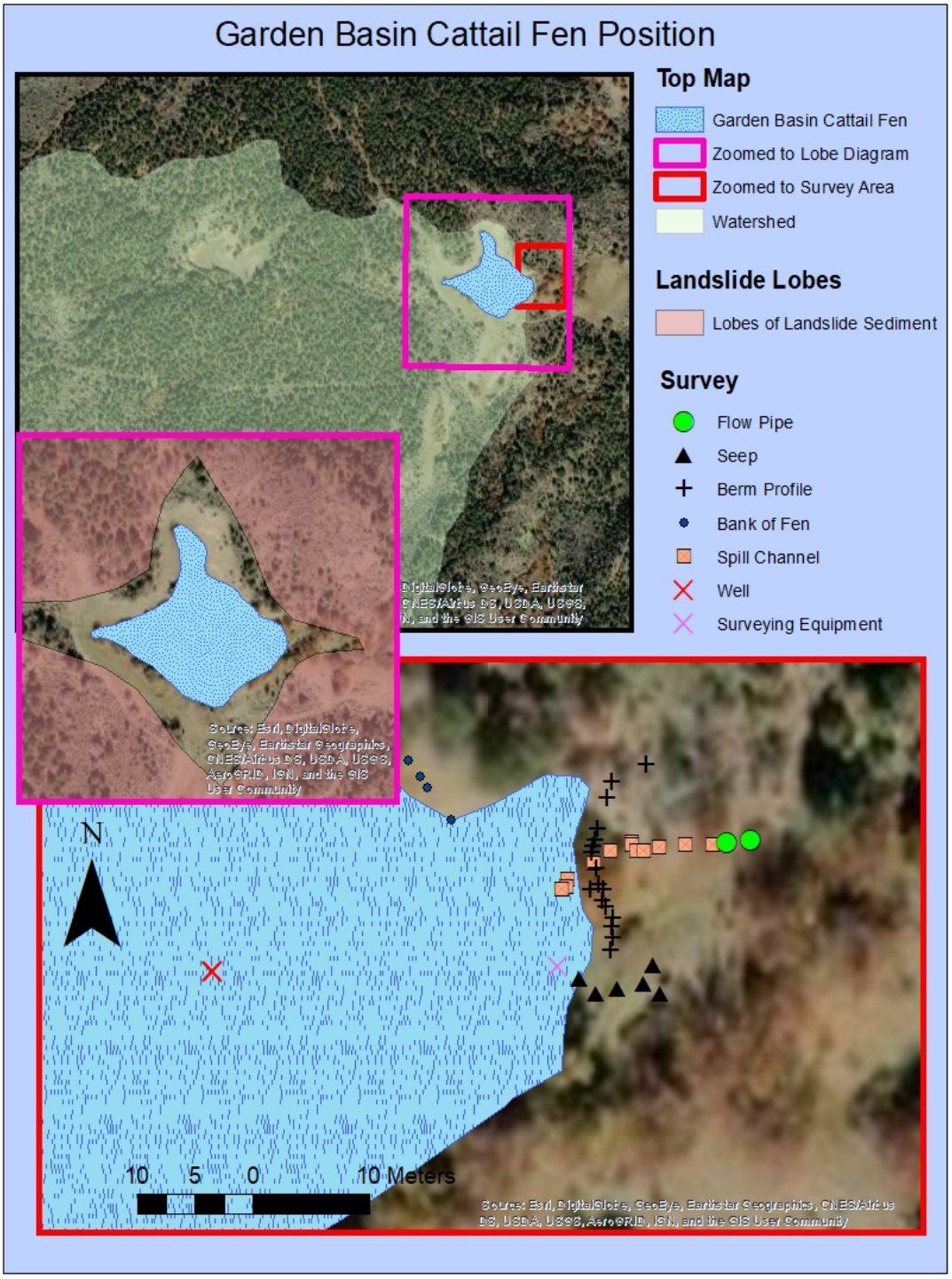

Figure 1.9 The map above depicts position of GBC fen in relation to its corresponding watershed, the hummocks/lobes of landslide material surrounding the fen, and the survey conducted at specific points on the east portion of the fen.

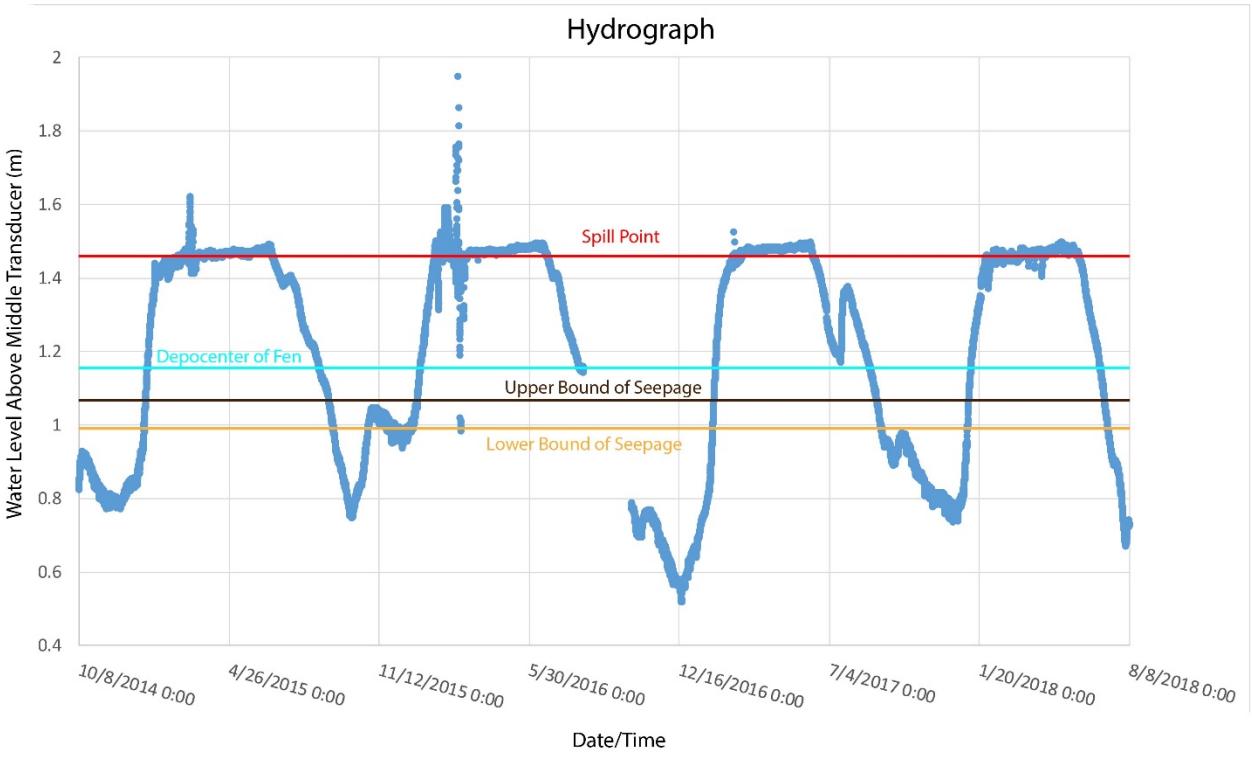

Figure 1.10 The above graph shows water levels in relation to the spill point, ground level, and seepage area. Notice the plateaus that trend along the spill point. These features are caused as the fen overflows, spilling water continuously through about 6 months of the year. The large dips between the plateaus are likely due to an increase (then decrease) in transpiration along with groundwater fluxes from snowmelt.

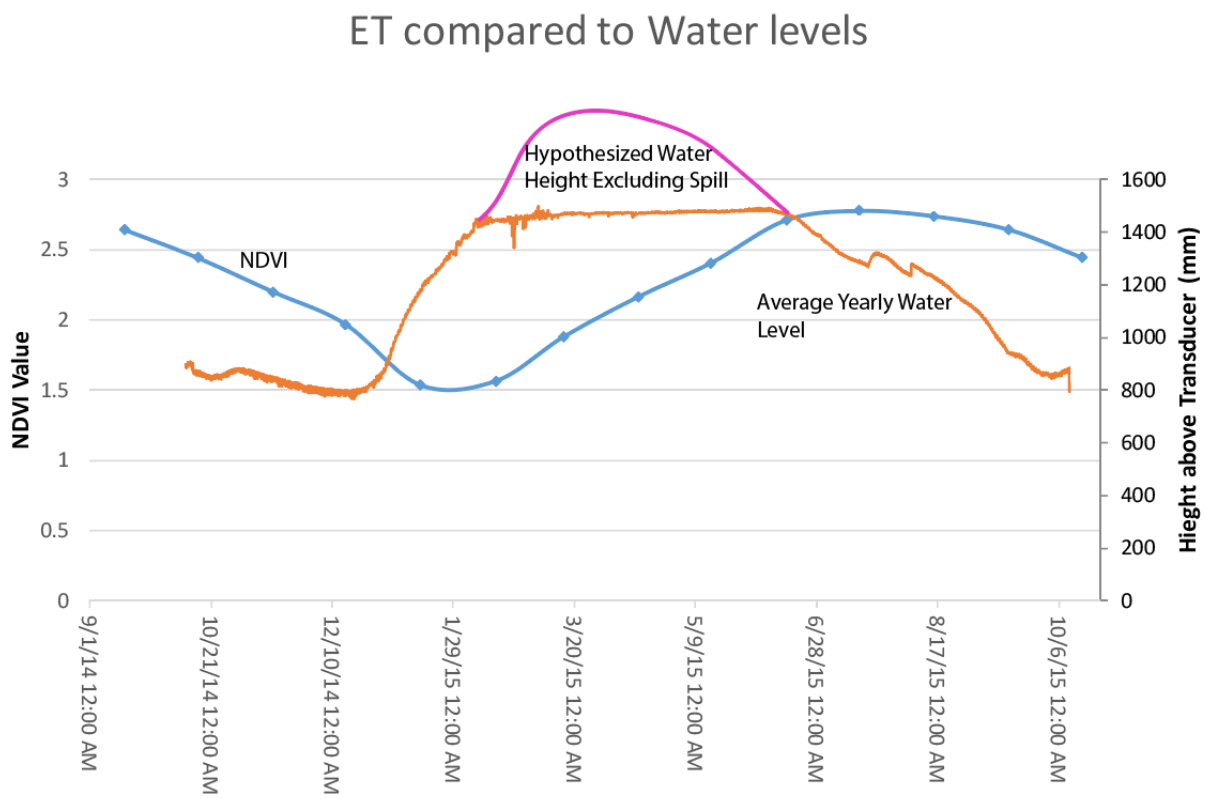

Figure 1.11 The simplified figure above shows the comparison of water levels to evapotranspiration calculated from NDVI data (NASA, 2016): Series 1 indicates estimated ET (standard error of ±.4) and the orange line shows average water level height from 2014 to 2018. Water levels begin to drop as evapotranspiration peaks, which may be due to a decrease in vegetation removing water from the subsurface. The water level then begins to increase as plants begin to shut down in the colder winter months. The yellow box indicates a period of time where input is needed to continue the plateau in water levels caused by spillage. If enough water was input during this period of time, the fen would likely become a pond year-round.

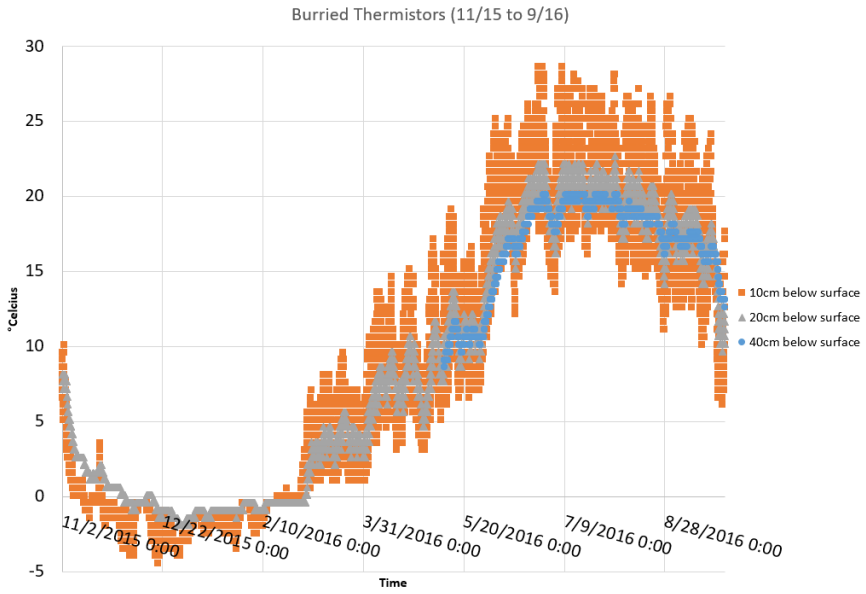

Figure 1.12 Thermistor values (°C) depicted vs. time. Note the decreased variability toward the yearly average.

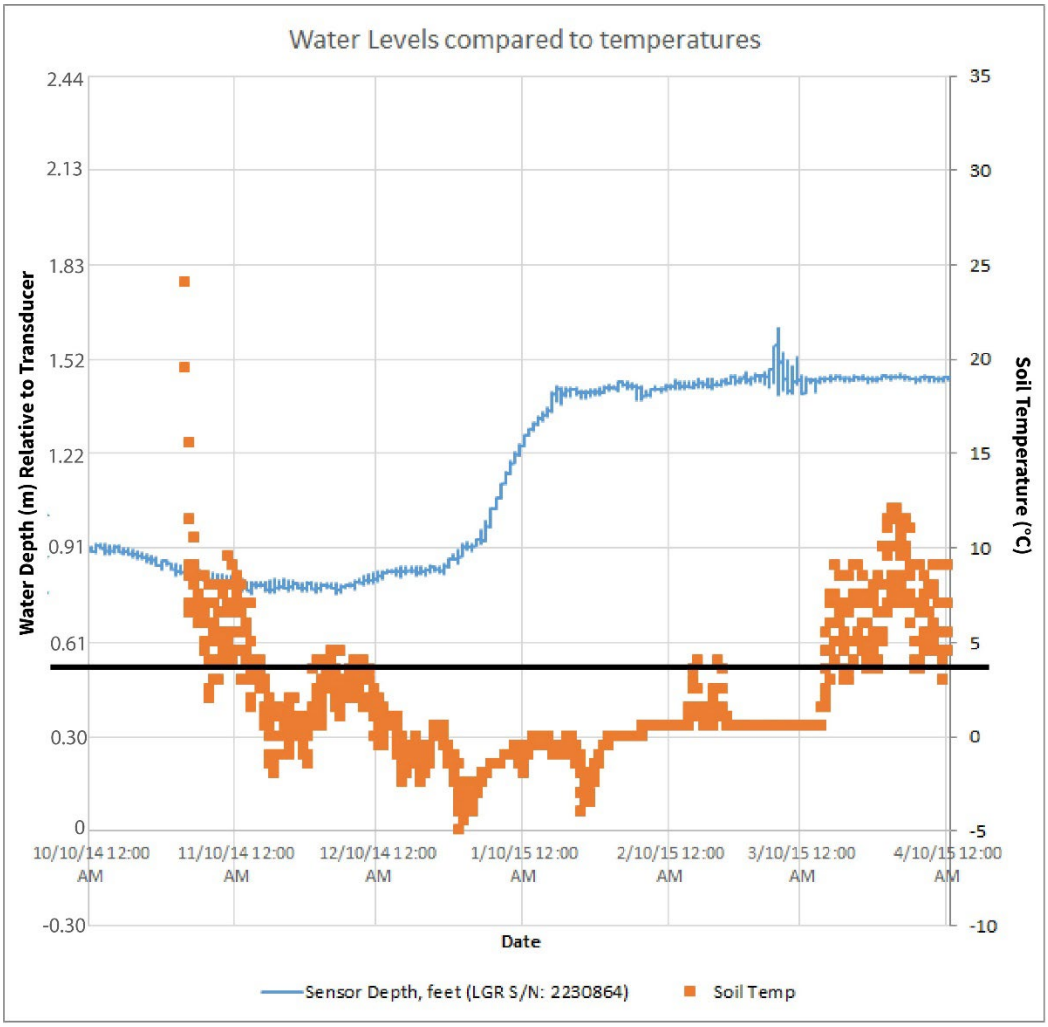

Figure 1.13 This figure depicts the relationship of piezometer data to soil temperatures at 20cm depth. The horizontal black line represents the boundary of 4.4*C which is linked to a significant decrease in Western Juniper transpiration (Miller, 2005). Notice that when temperatures decrease below this line around 11/10/14, there the negative slope of the transducer data becomes shallower. As the temperatures decrease further, the trend becomes increasingly positive, likely due to a lack of thirsty plants taking up groundwater.

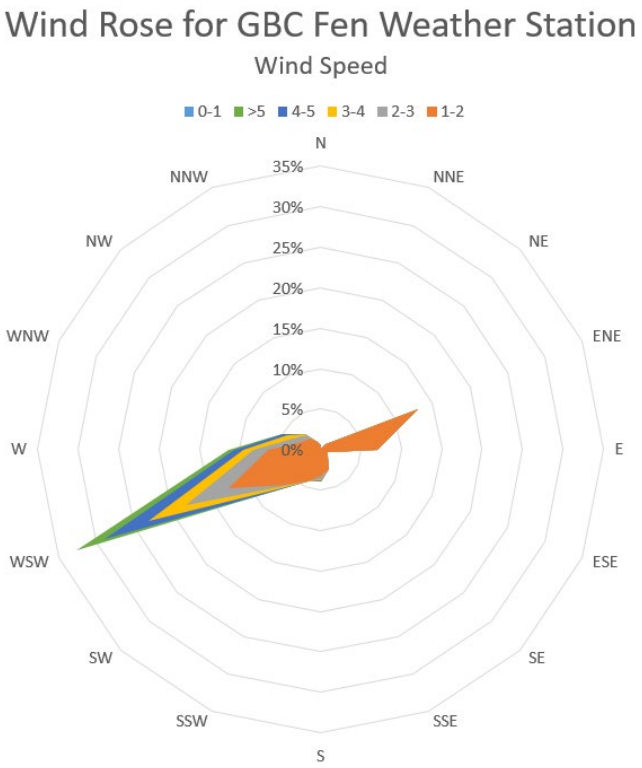

Figure 1.14 This is a rose diagram constructed from wind measurements from the Davis Pro Weather Station located at GBC fen.

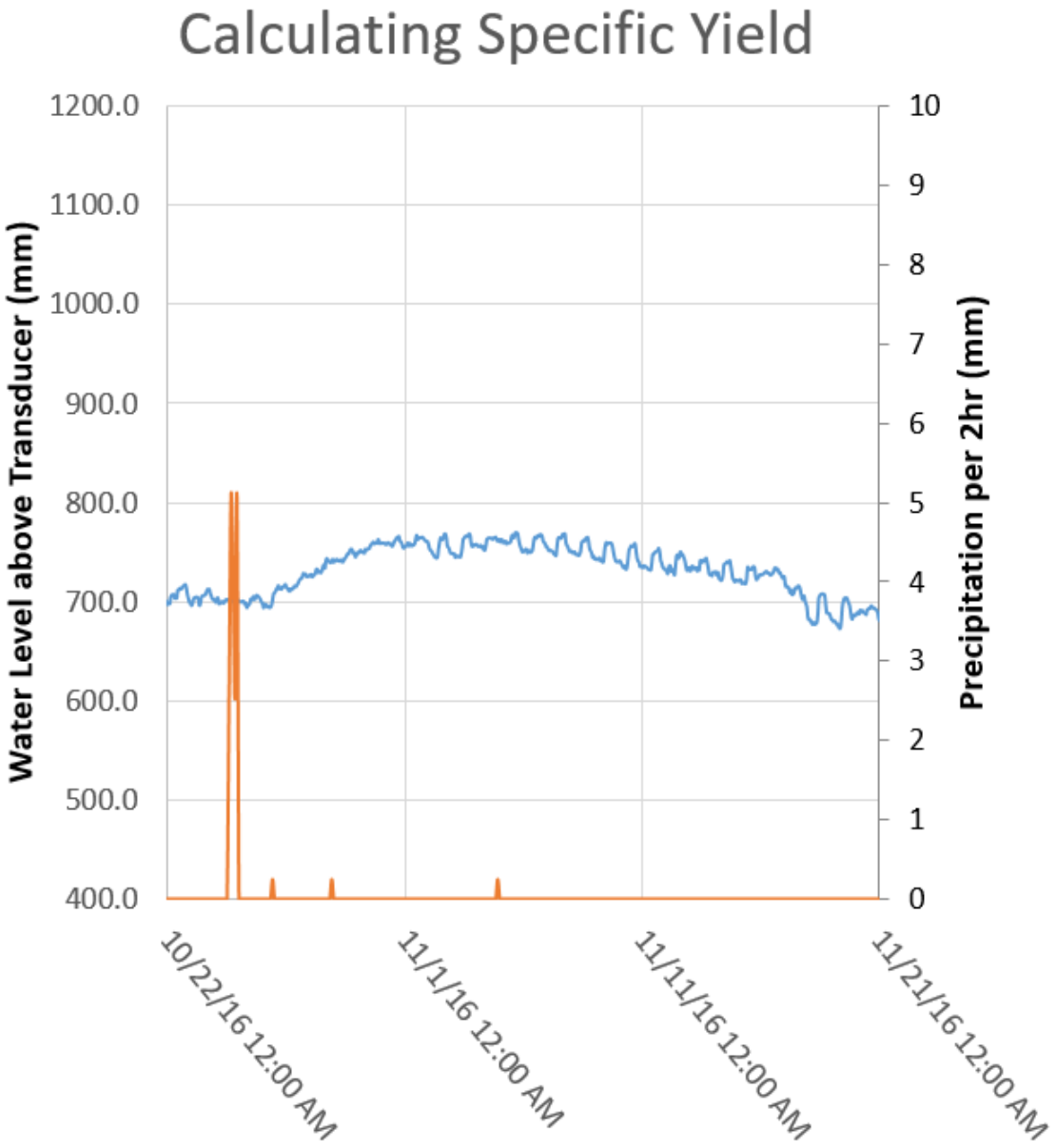

Figure 1. 4 The graph above shows the relationship between a rain event occurring on 7/19/2017 (as shown by the weather station data in green) and the water level fluctuation afterward (as shown by the piezometer data in blue.

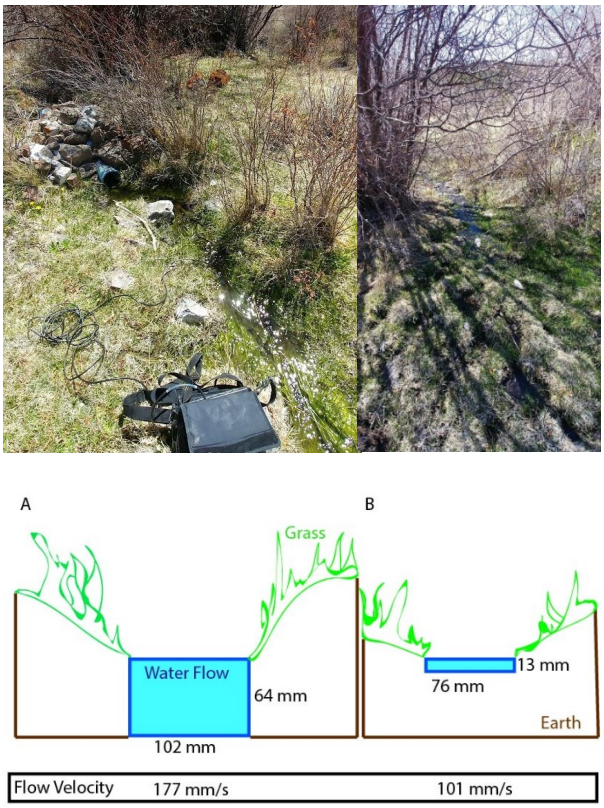

Figure 1.16 This figure shows the cross-section of the flow of water (A) leaving the fen through the spill point and from the combination of seepage points into one stream. Below each cross-section is the flow velocity measured at each location.

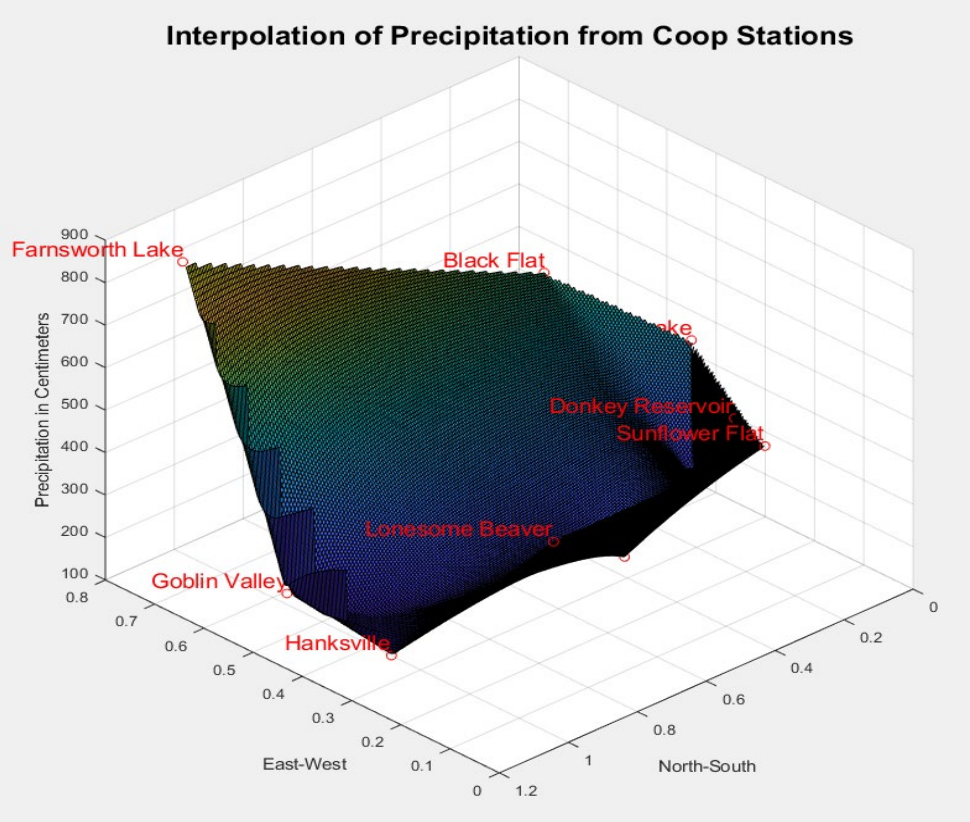

Figure 1.17 The image above was created in MATLAB using the 'griddata' and 'mesh' functions. Precipitation Data and Coordinates were used to interpolate precipitations values for the area. Notice the large dip in the interpolation from east-west, where precipitation values are much lower. This may indicate a rain shadow from Geyser Peak, located just to the west of GBC fen.

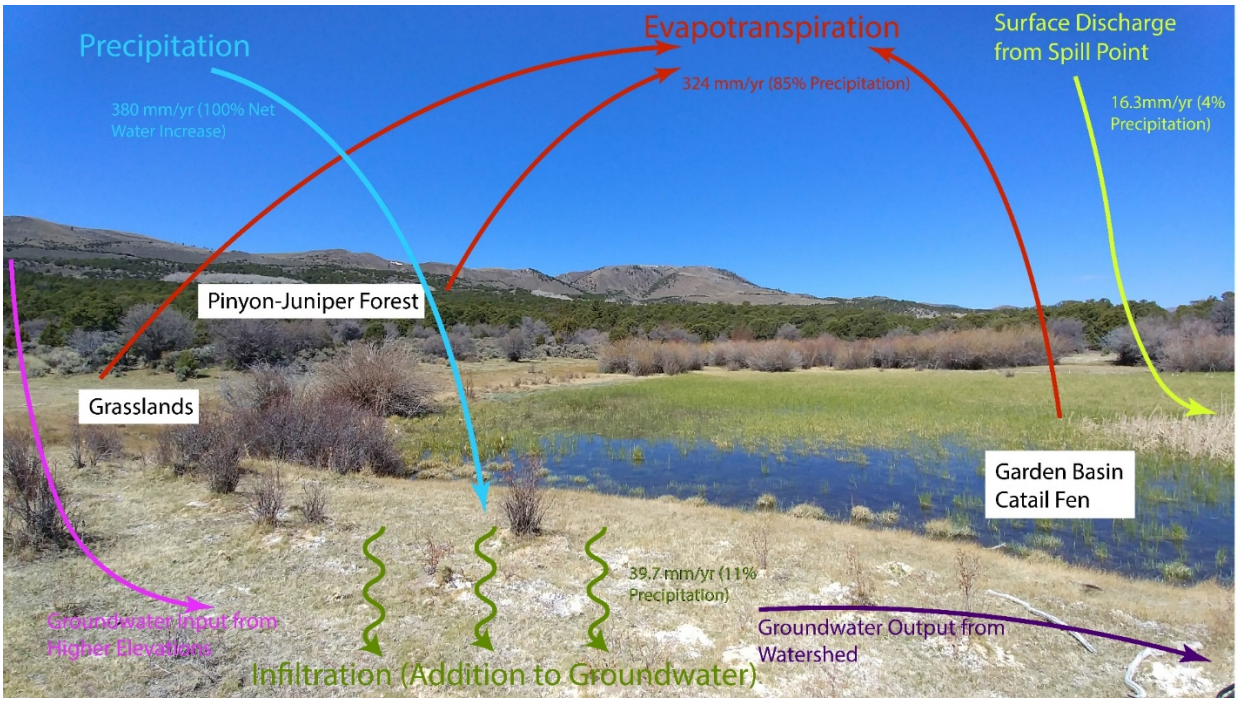

Figure 1.18 Simplified diagram showing the relationship between the variables of the watershed's water budget mentioned in Eq. 1. It is assumed that there is no net change in water storage.

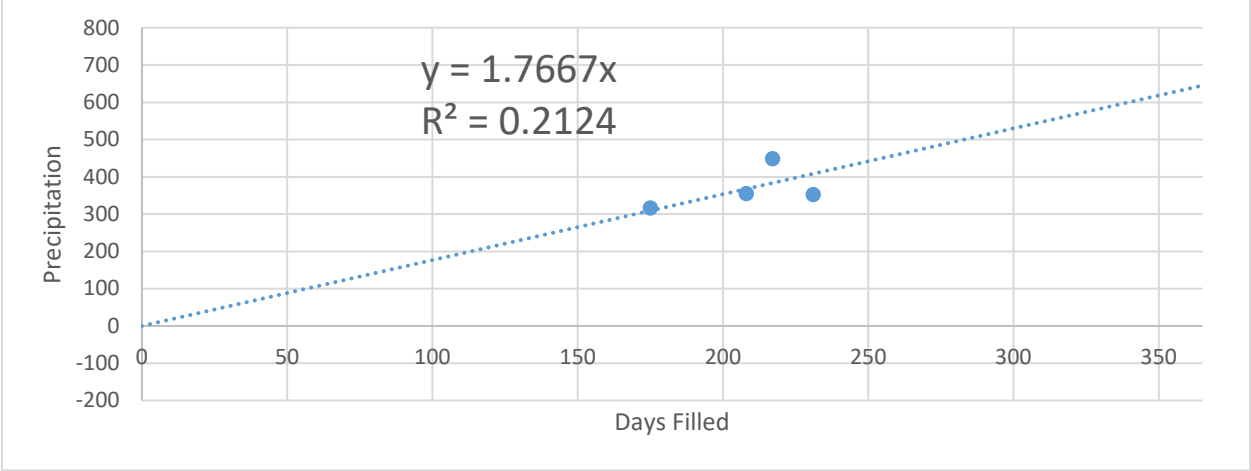

Figure 1.19 The relationship between the number of days each year with water above ground versus local (PRISM, 2019) for the GBC fen. Data include 2015-2018. Note that the regression is forced through the origin on the assumption that in the absence of precipitation there could be no standing water. See text for discussion.

CHAPTER 2

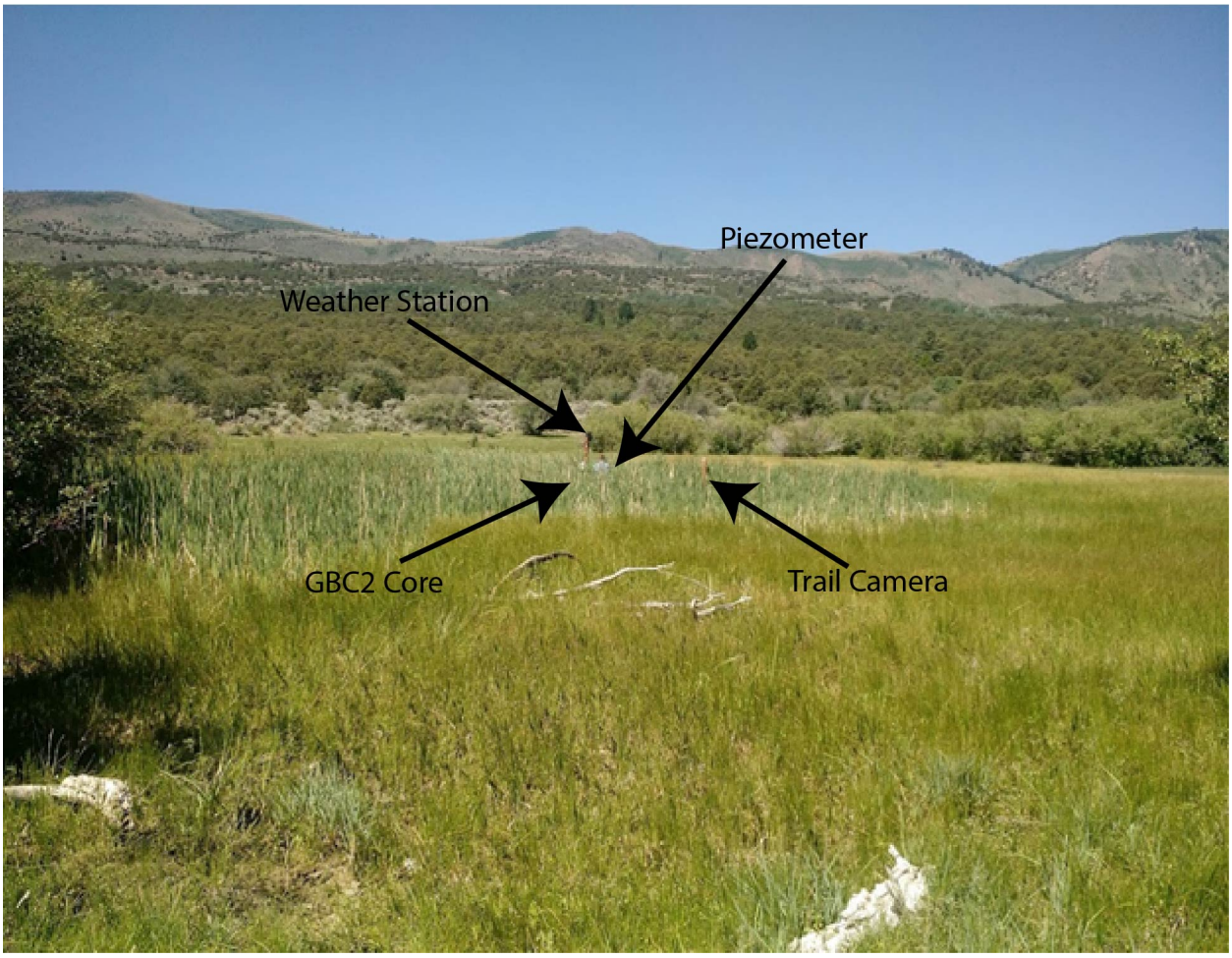

Figure 2. 1 This is an image looking west from the spill point (Fig. 1.6). Notice the cattails in the deepest part of the fen, which retains surface water longer than the rest of the body. Long grasses grow around this the cattails as water levels decrease.

Figure 2. 2 View of the GBC fen looking to the NNE. Note the position of the two cores.

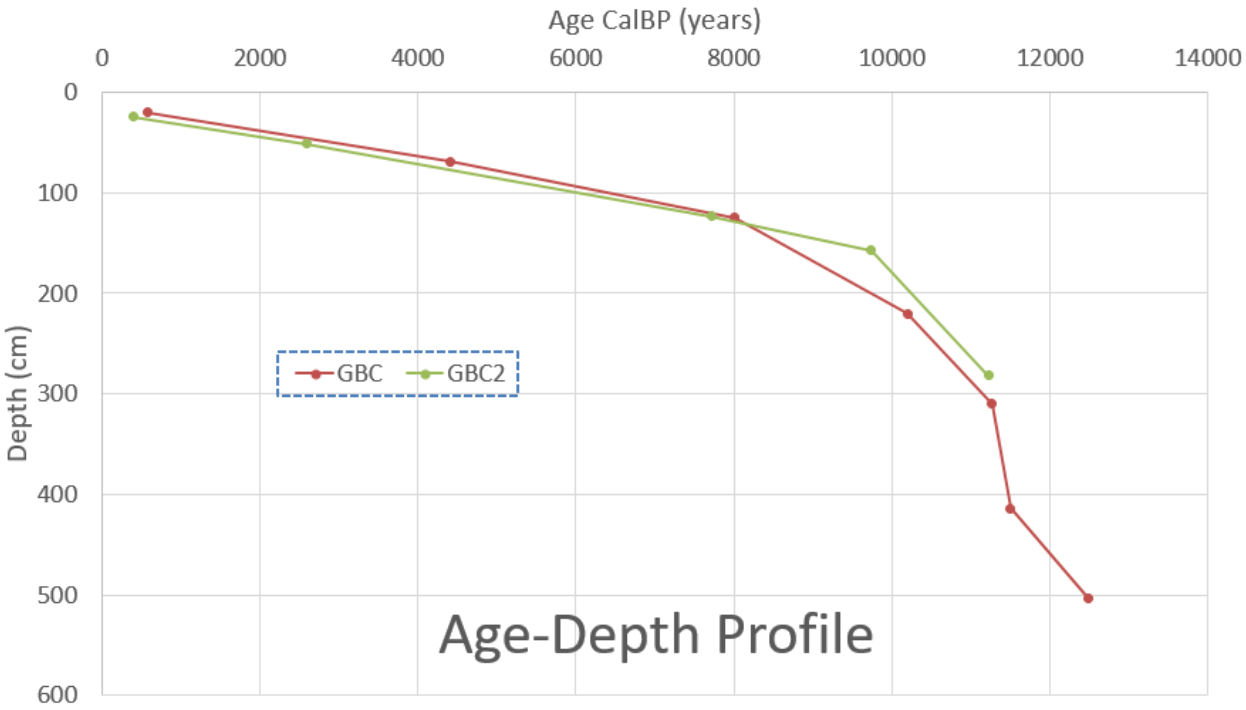

Figure 2. 3 Age-Depth Profile of both GBC core (Shurtliff et al., 2017) and GBC2 core.

Figure 2.4 The following six images depict the core stratigraphy of GBC2 core. Eight samples removed from the core for carbon ages (black stars) and ESEM imaging (red circles). Note a general trend in the core from black to grey to green to brown with a black cap.

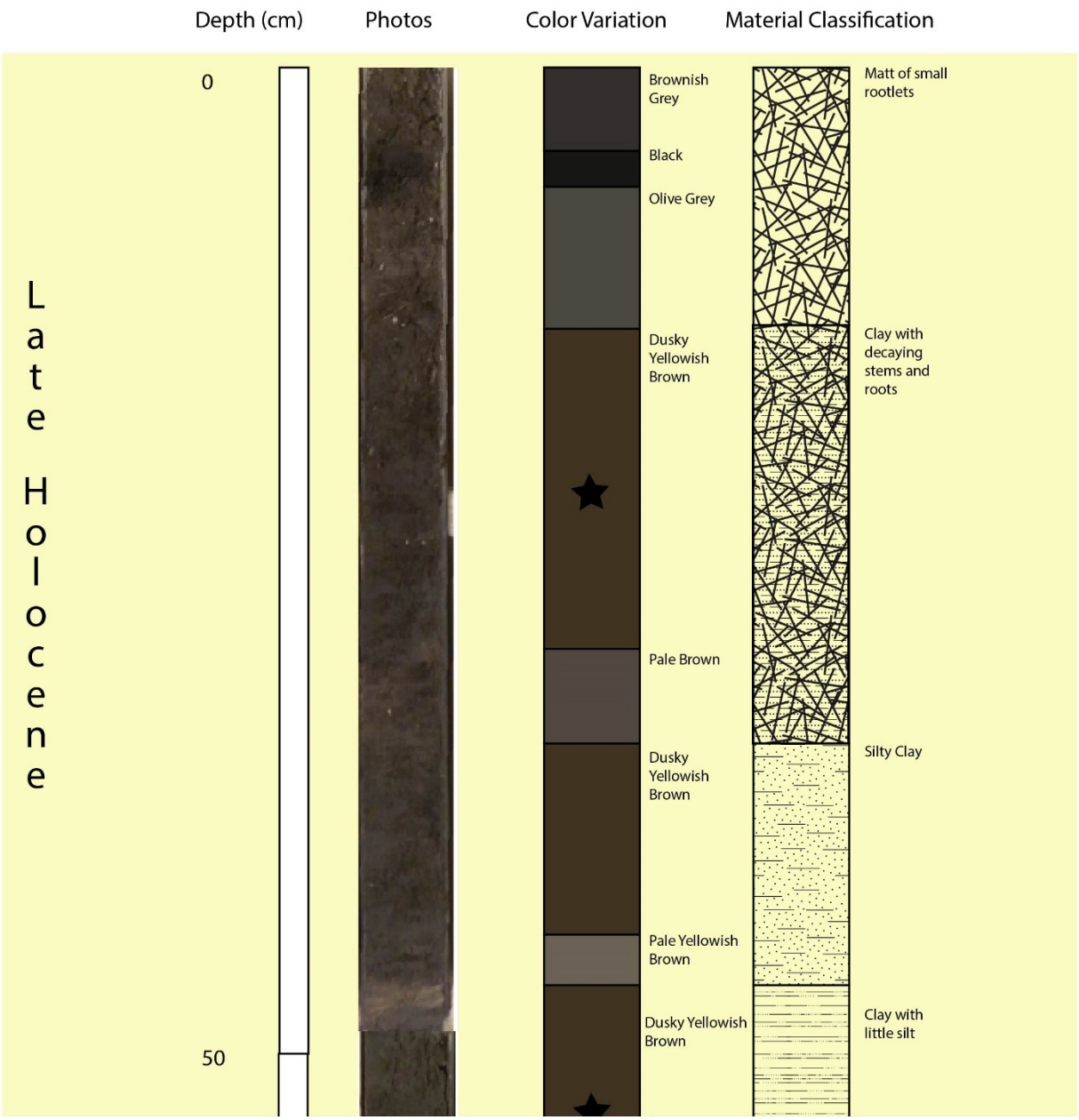

Figure 2.4 continued (Middle Holocene)…

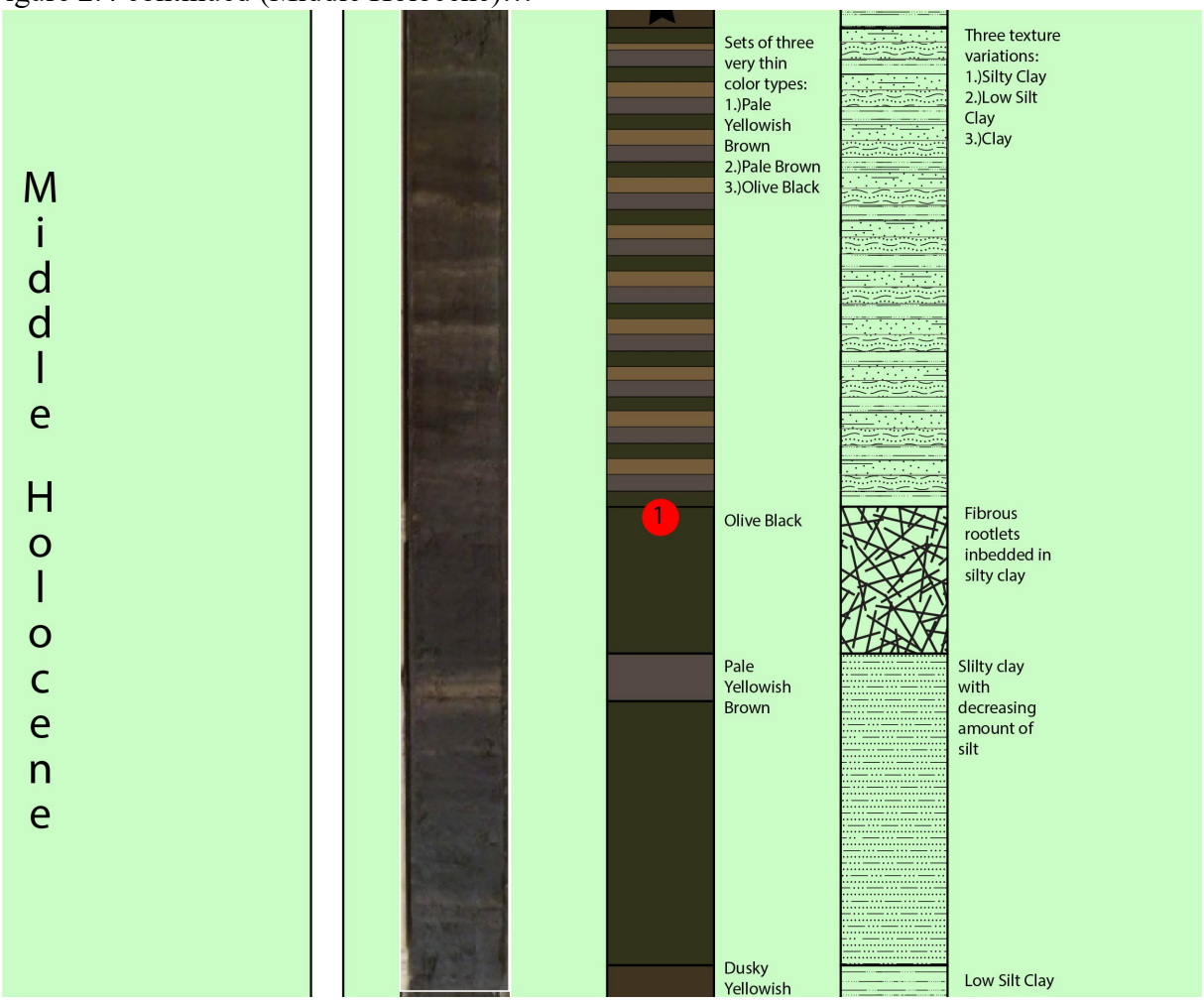

Figure 2.4 continued (Early Holocene)…

Figure 2.4 continued (Pleistocene of Holocene Transition)…

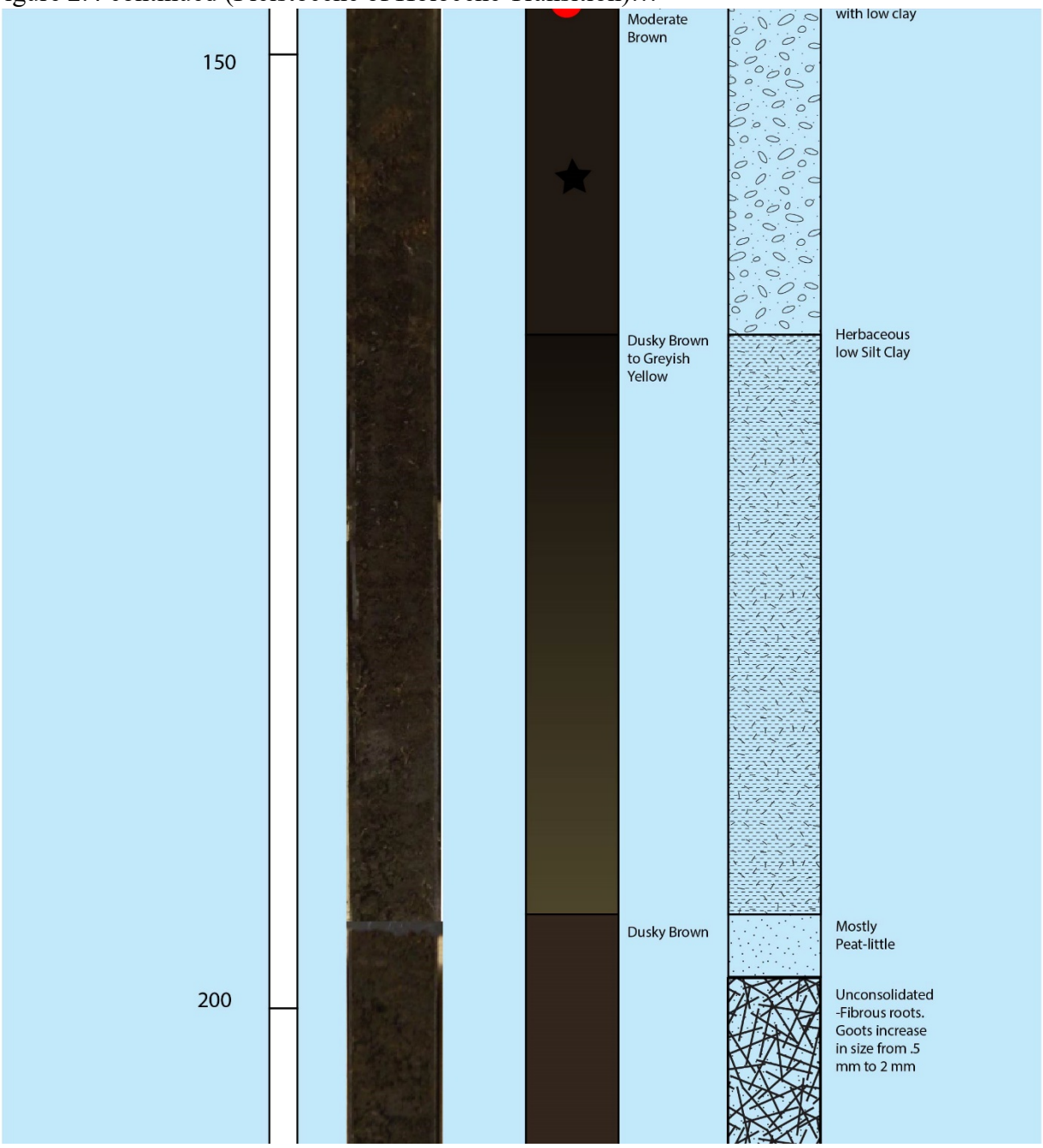

Figure 2.4 continued (Pleistocene of Holocene Transition)…

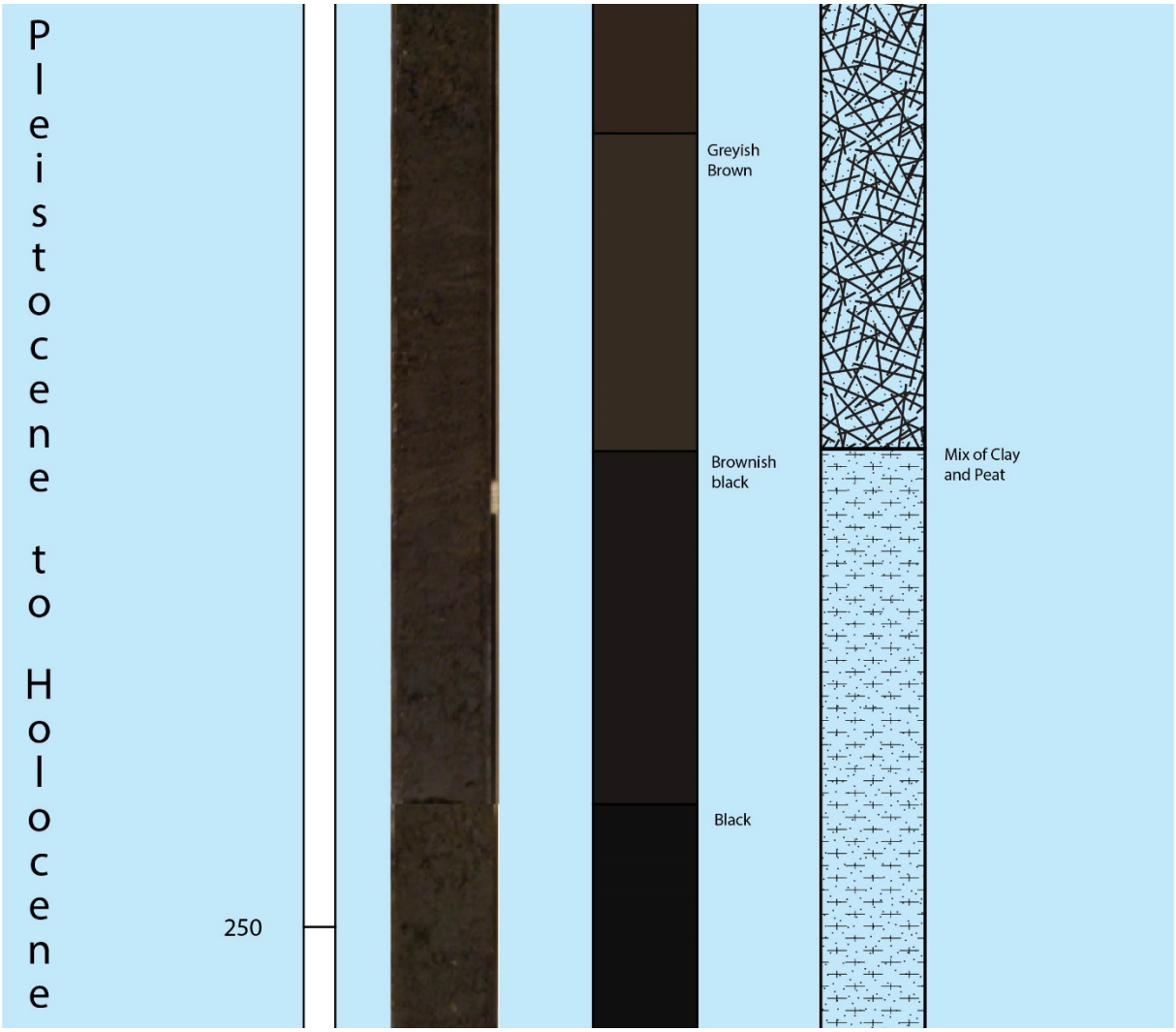

Figure 2.4 continued (Pleistocene of Holocene Transition/Younger Dryas)…

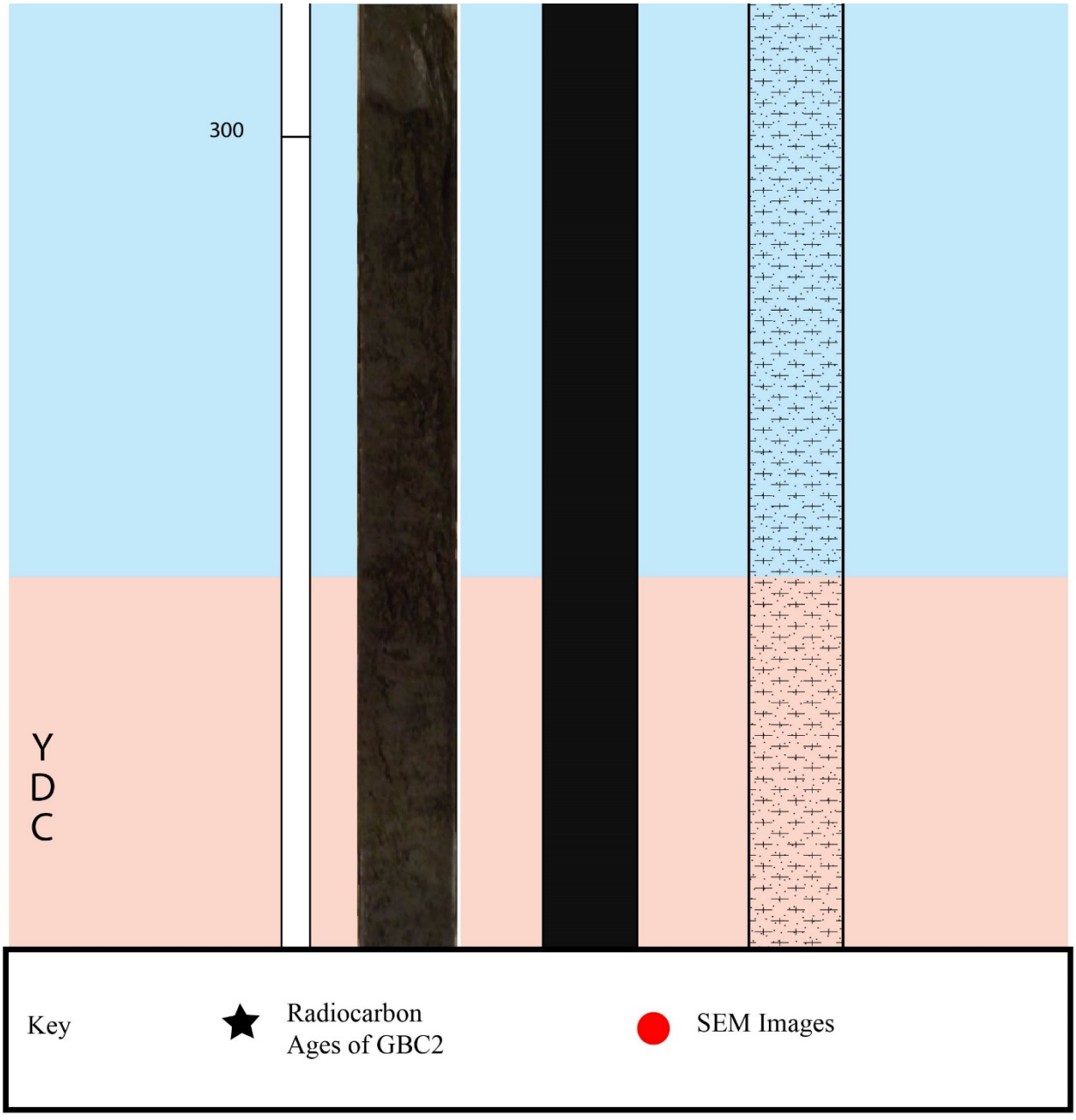

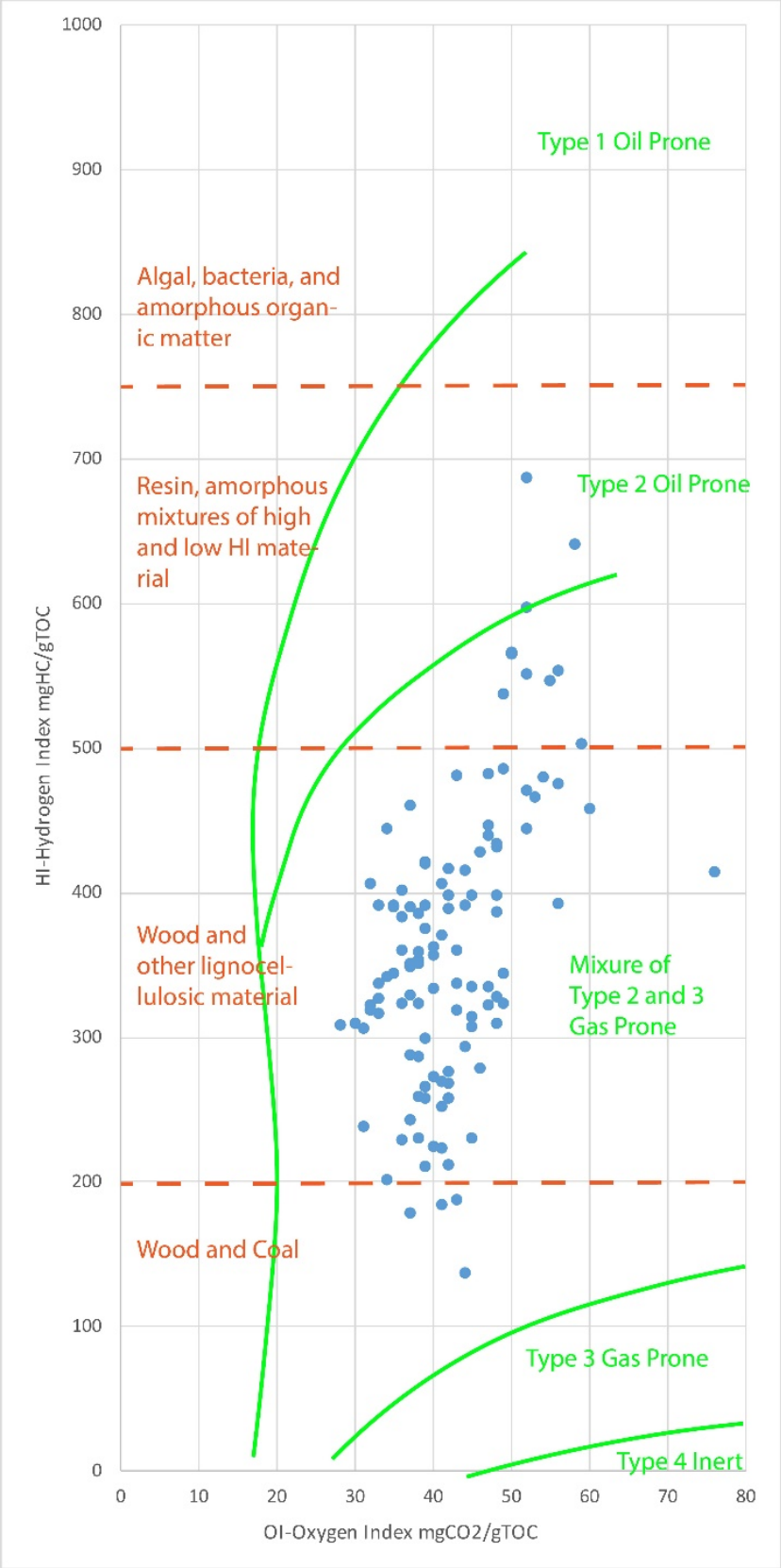

Figure 2.5 Classification of Kerogen Types from Pyrolysis samples (HI values) of GBC2 core. Modified from Hudson et al. (2019).

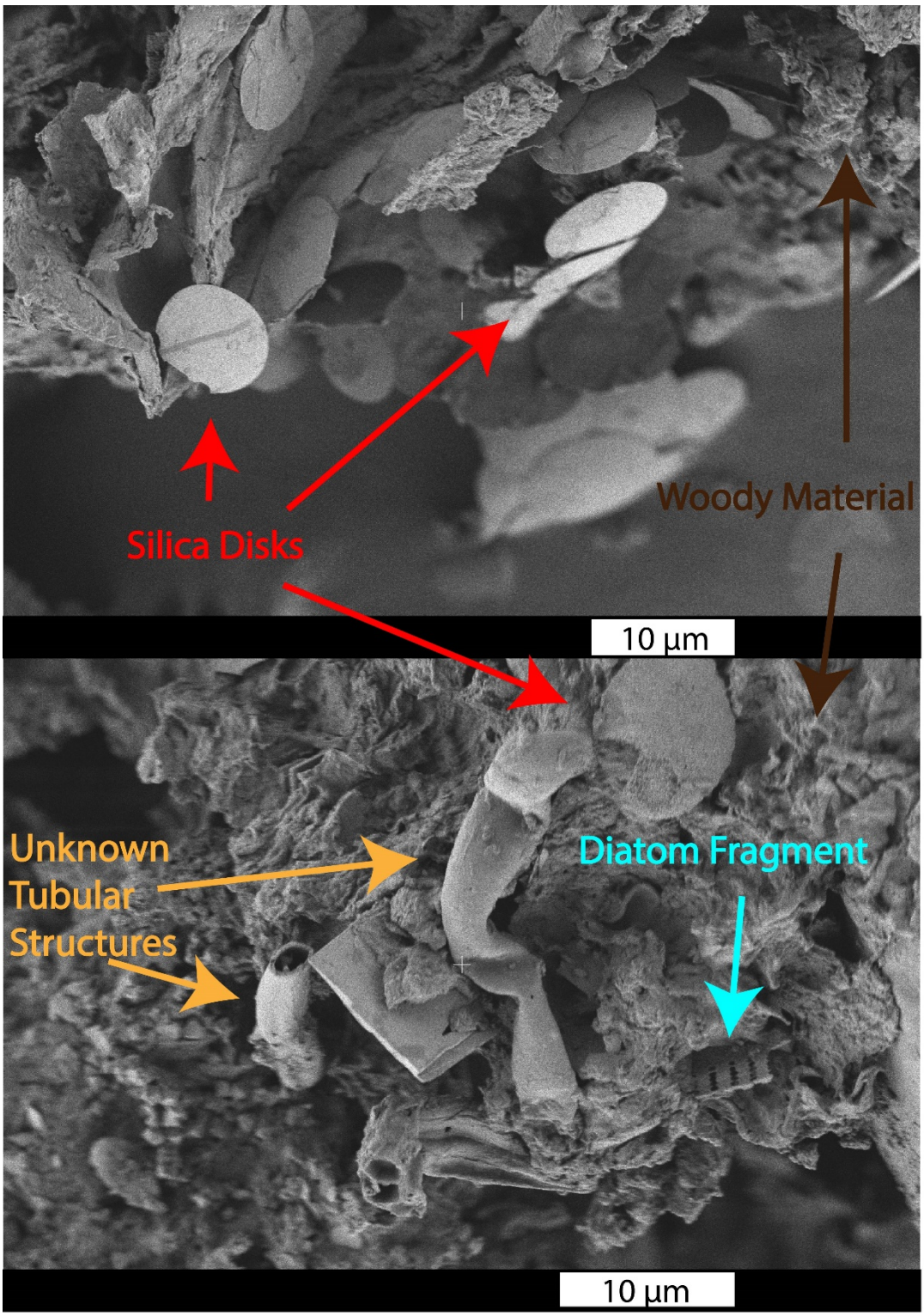

Figure 2.6 Secondary electron SEM of sediment at a depth of 230 cm (~10.7ka) in the GBC2 core, indicating the dominance of organic debris.

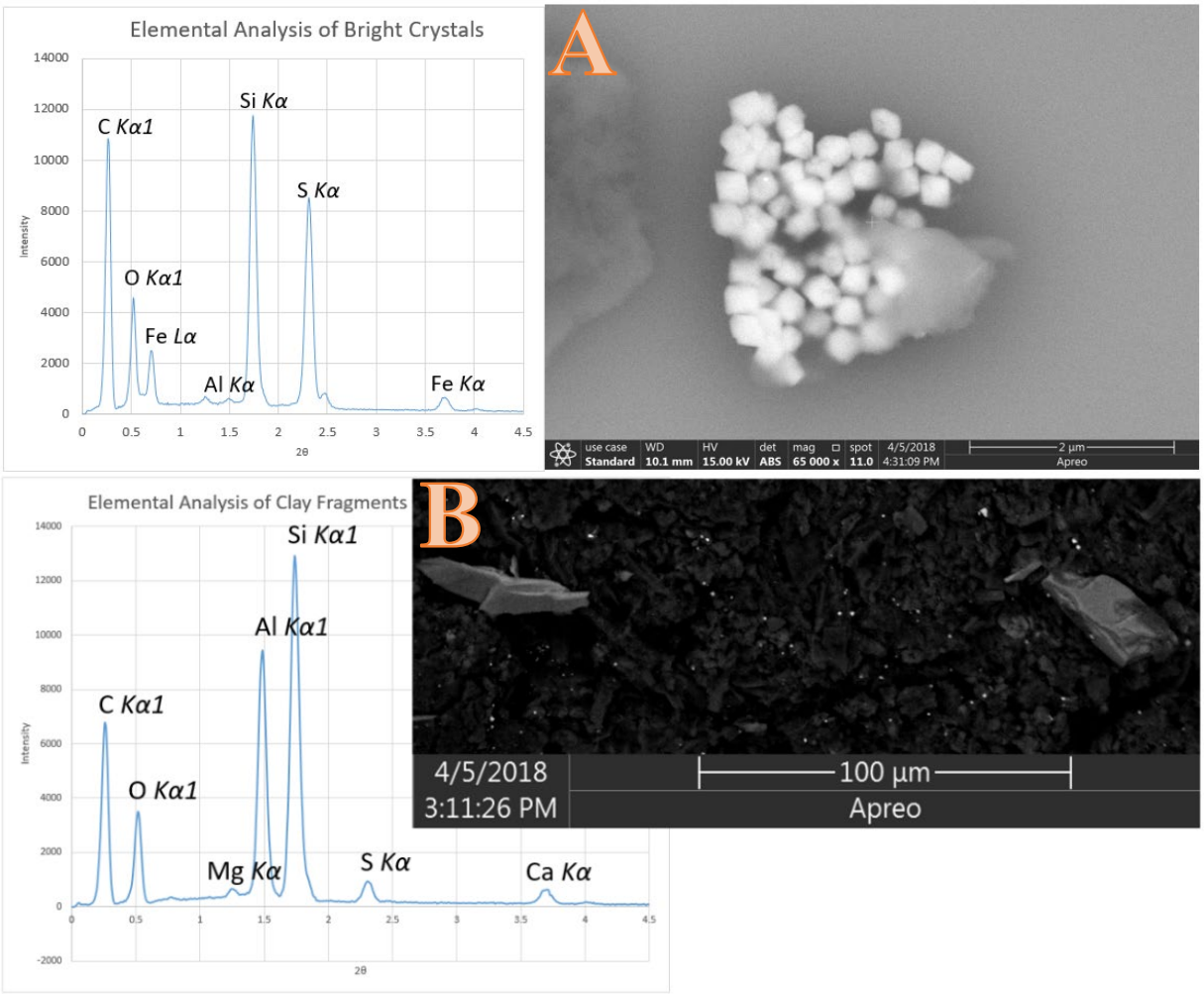

Figure 2.7 Secondary-electron SEM image of sediment at 148 cm depth (~9.6 ka) of GBC core 2. Image A depicts bright, flat objects high in aluminum, suggesting clays. The Large spikes in carbon (C) are from carbon tape used for mounting. Image B shows a close up view of some of the brighter specks similar to those seen in image A. The presence of Iron (Fe) and Sulfur (S) suggest iron sulfides such as pyrite.

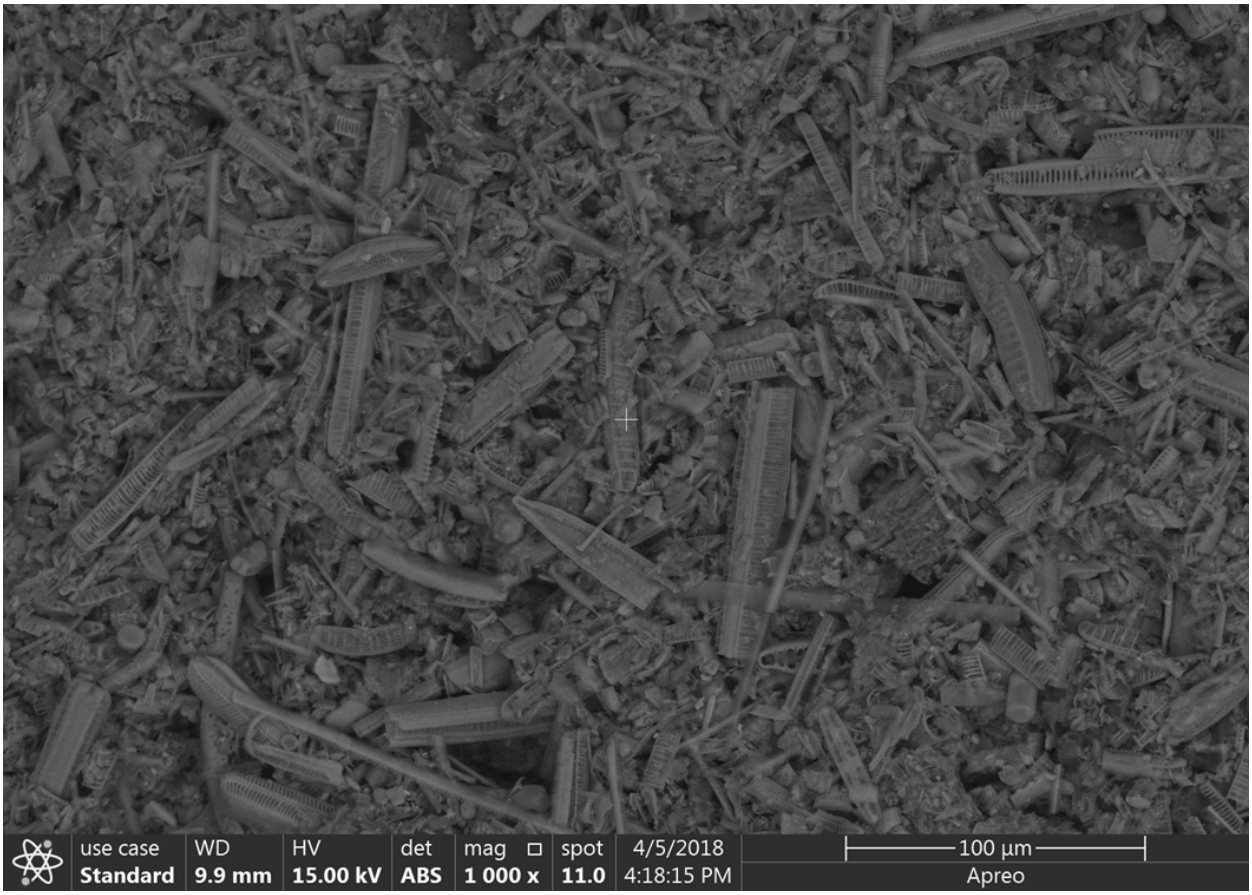

Figure 2.8 Secondary-electron SEM image of sediment at 68 cm depth (~4.1 ka) of GBC core 2 showing abundant diatom debris, consistent with energy-dispersive spectra (not shown) indicating the material is nearly pure SiO_2.

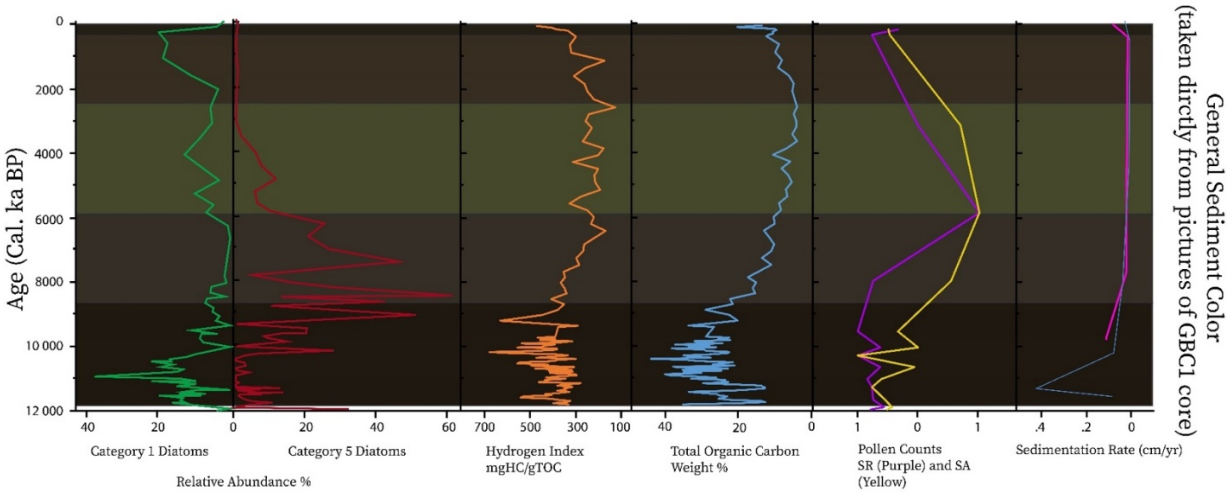

Figure 2. 9 Total Organic Carbon (TOC) from pyrolysis analysis of fen material visually compared to other know data sets from GBC fen. Note the general trend from ~11.5 ka BP to more recent times with higher and more variable values, transitioning to a shallow trough, and finally ending in a sharp peak. Hydrogen Index, precipitation, and diatom values show striking seminaries to TOC. Also note, shallow water and terrestrial sediment (corresponding to Fig. 2.8) occur in the shallow valley while deeper-water sediment was seen in the later and earlier peaks.

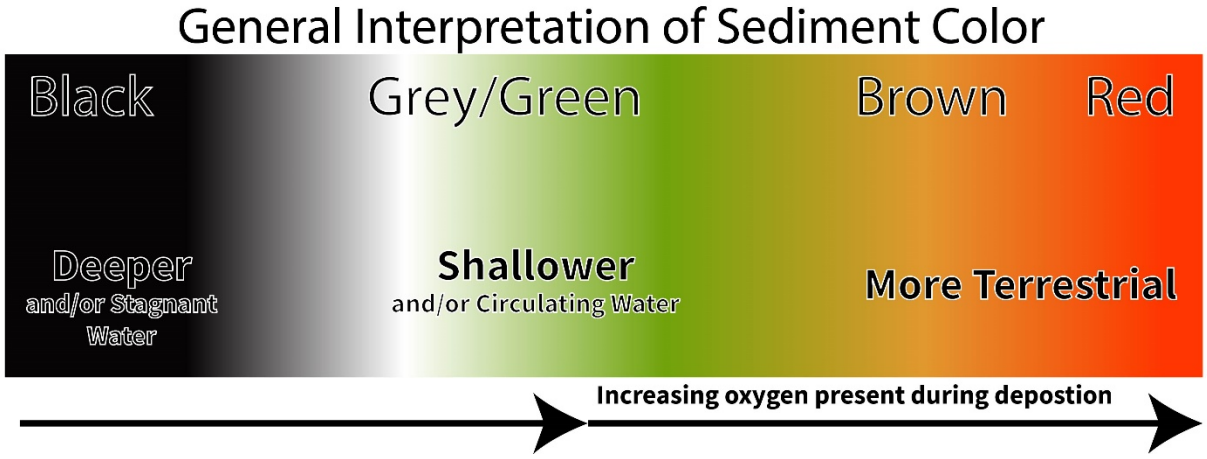

Figure 2. 10 The figure above shows how color variations in sediment can be an indication for the depositional environment (Modified from Fitcher, 2015).

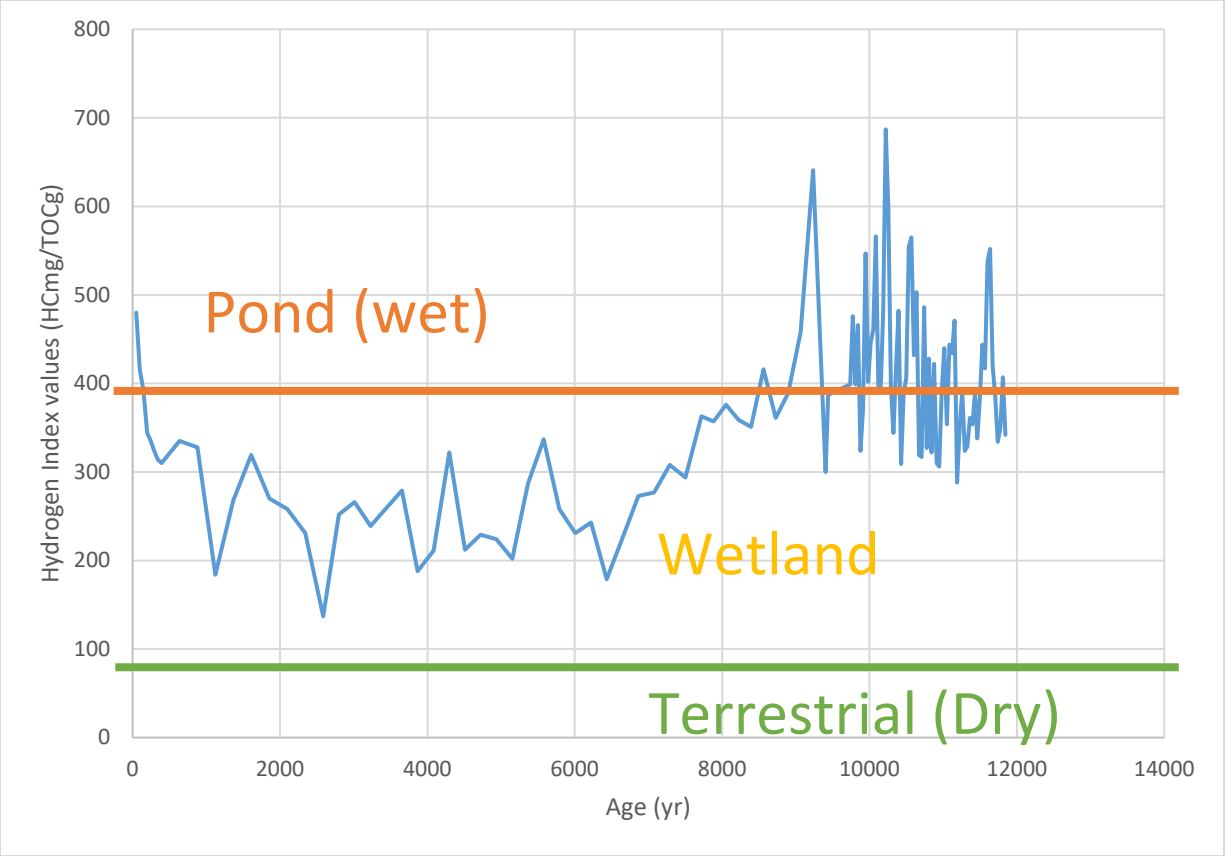

Figure 2.11 Hydrogen index values plotted within pond and wetland environments as suggested by Bonnefille (1996). Note the oscillations varying between wetland and pond environments earlier, whereas wetland conditions dominate after ~9 ka BP.

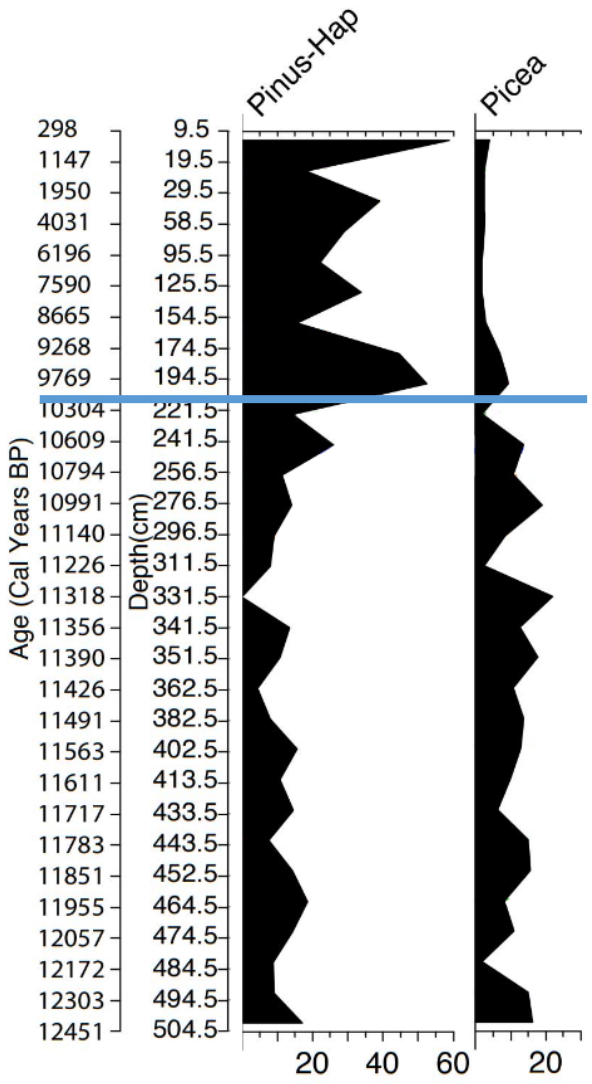

Figure 2.12 The figure above shows pollen counts for Pinus-Hap (indicator of PJ forests) and Picea (indicator for spruce forests) (Shurtliff et al., 2017). These two pollen charts seem to have opposing trends. About 9,500 to 10,500 years ago there seems to have been a shift from an area higher in spruce and lower in PJ to an area higher in PJ and lower in spruce.

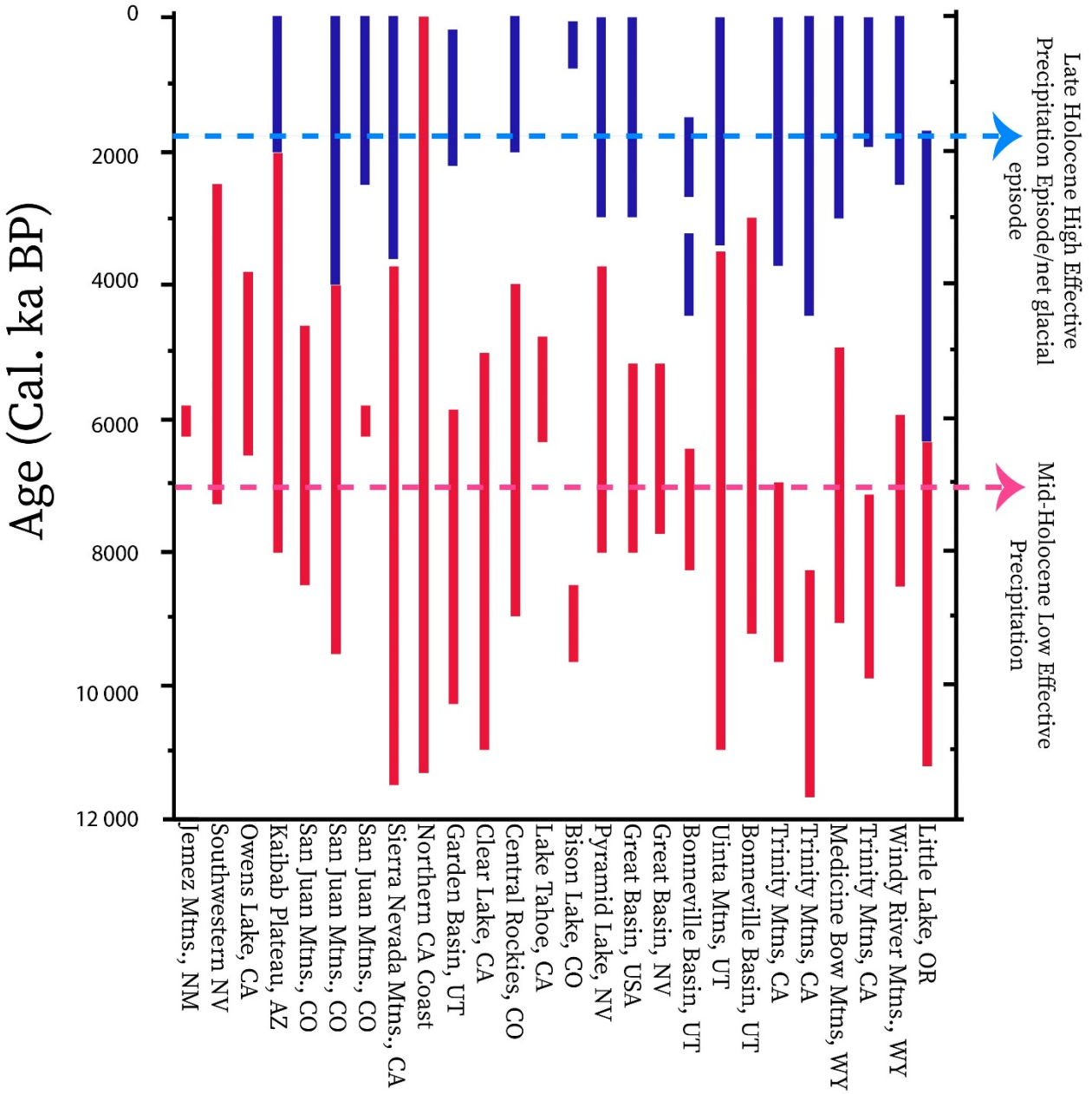

Figure 2. 13 Compilation of Climate proxies throughout the western US, modified from Shurtliff et al. (2017). Note the midpoints of both low (earlier) and higher (later) effective moisture events.

TABLES (Non-digitized)

Table 1 Dimensions of the well within GBC fen, as well as describing the location of pressure transducers.

Well Dimensions	**(cm)**	**Pressure Transducer**	**Distance Below Surface (cm)**
Stickup	**81.28**	**Top**	**-42.545**
Diameter	**5.08**	**Middle**	**105.41**
		Bottom	**275.59**

Table 2 List of inputs and outputs to the watershed system as suggested by the water budget (Eq. 2).

Precipitation (PRISM, 2019) m^3/yr	**Surface Outflow m^3/yr**	**Evapotranspiration m^3/yr**	**Infiltration m^3/yr**
380900	16675.8	323678	40601

Table 3 Carbon ages of sediment taken from GBC2 core (Fig. 2.4) and processed using Calib 7.1 software.

Sample ID	Radiocarbon Age (YBP)			Corrected Median Years using Calib 7.1 (Calendar Years BP)	Depth (cm)
0-2 45cm GBC2	-4586	±	22	392	24
2-4 25cm GBC2	-10641	±	23	2586	51
4-6 43cm GBC2	-17713	±	26	7717	123
6-8 30cm GBC2	-19674	±	26	9739	157
10-12 44cm GBC2	-24378	±	27	11223	282

APPENDIX (Non-digitized)

Table.A.1 Data collected from an elevation survey performed in the area of GBC fen.

Landmark	UTM zone	UTM easting	UTM northing	relative elevation (reported in meters)	easting (reported in ft.)	northing (reported in ft)
Reference Location	**12S**	**463519**	**4263159**	**30.48**	**0**	**0**
Base of well	**12S**	**463489.18**	**4263158.54**	**29.77**	**-97.83**	**-1.50**
Top of well casing	**12S**	**463489.22**	**4263158.51**	**30.61**	**-97.69**	**-1.60**
channel	**12S**	**463519.78**	**4263166.15**	**30.05**	**2.57**	**23.45**
channel	**12S**	**463522.03**	**4263167.43**	**30.06**	**9.95**	**27.64**
channel	**12S**	**463523.48**	**4263168.46**	**30.09**	**14.68**	**31.05**
channel	**12S**	**463525.40**	**4263169.19**	**30.07**	**20.99**	**33.45**
channel	**12S**	**463527.75**	**4263168.76**	**30.00**	**28.70**	**32.04**

channel	**12S**	**463530.01**	**4263169.00**	**29.95**	**36.13**	**32.82**
channel	**12S**	**463532.29**	**4263169.02**	**29.89**	**43.60**	**32.88**
channel	**12S**	**463525.34**	**4263169.03**	**30.07**	**20.79**	**32.89**
channel	**12S**	**463525.82**	**4263168.54**	**30.07**	**22.37**	**31.31**
channel	**12S**	**463526.39**	**4263168.47**	**30.05**	**24.26**	**31.06**
channel	**12S**	**463519.41**	**4263165.35**	**30.05**	**1.35**	**20.82**
channel	**12S**	**463519.67**	**4263165.54**	**30.08**	**2.19**	**21.46**
channel	**12S**	**463519.27**	**4263165.32**	**30.06**	**0.89**	**20.75**
bank misc.	**12S**	**463506.06**	**4263176.02**	**30.20**	**-42.47**	**55.85**
bank misc.	**12S**	**463507.11**	**4263174.63**	**30.25**	**-39.00**	**51.28**
bank misc.	**12S**	**463507.72**	**4263173.78**	**30.21**	**-37.02**	**48.50**
bank misc.	**12S**	**463509.80**	**4263171.05**	**30.12**	**-30.18**	**39.54**
dike profile	**12S**	**463522.26**	**4263167.02**	**30.07**	**10.69**	**26.32**
dike profile	**12S**	**463521.82**	**4263168.37**	**30.21**	**9.26**	**30.74**
dike profile	**12S**	**463522.00**	**4263168.94**	**30.36**	**9.83**	**32.62**
dike profile	**12S**	**463522.13**	**4263169.39**	**30.45**	**10.27**	**34.08**
dike profile	**12S**	**463522.42**	**4263170.36**	**30.75**	**11.23**	**37.26**
dike profile	**12S**	**463523.18**	**4263172.87**	**30.79**	**13.71**	**45.52**

dike profile	**12S**	**463523.58**	**4263174.22**	**30.82**	**15.04**	**49.92**
dike profile	**12S**	**463521.77**	**4263165.29**	**30.31**	**9.10**	**20.64**
dike profile	**12S**	**463522.47**	**4263165.69**	**30.19**	**11.40**	**21.94**
dike profile	**12S**	**463522.86**	**4263165.35**	**30.34**	**12.66**	**20.82**
dike profile	**12S**	**463522.81**	**4263164.39**	**30.54**	**12.51**	**17.67**
dike profile	**12S**	**463523.14**	**4263163.90**	**30.52**	**13.57**	**16.08**
dike profile	**12S**	**463523.69**	**4263162.99**	**30.31**	**15.38**	**13.10**
dike profile	**12S**	**463523.59**	**4263162.22**	**30.14**	**15.05**	**10.56**
dike profile	**12S**	**463523.69**	**4263161.32**	**29.92**	**15.38**	**7.62**
dike profile	**12S**	**463523.49**	**4263160.33**	**29.93**	**14.73**	**4.35**
dike profile	**12S**	**463526.60**	**4263175.68**	**30.94**	**24.93**	**54.72**
dike profile	**12S**	**463526.60**	**4263175.69**	**30.94**	**24.94**	**54.74**
seep	**12S**	**463520.88**	**4263157.97**	**29.67**	**6.16**	**-3.39**
seep	**12S**	**463522.30**	**4263156.72**	**29.45**	**10.83**	**-7.47**
seep	**12S**	**463524.09**	**4263157.06**	**29.23**	**16.69**	**-6.38**
seep	**12S**	**463526.39**	**4263157.47**	**29.17**	**24.23**	**-5.02**
seep	**12S**	**463527.17**	**4263159.09**	**29.28**	**26.81**	**0.30**
seep	**12S**	**463527.86**	**4263156.74**	**29.01**	**29.06**	**-7.41**

flow pipe	**12S**	**463533.58**	**4263169.20**	**29.79**	**47.84**	**33.46**
flow pipe	**12S**	**463535.58**	**4263169.46**	**29.79**	**54.38**	**34.33**

Table.A.2 Duration of spilling and standing water.

Fen spill starts	**Fen spill ends**	**Days spilled**
January 17, 2015	June 21, 2015	155
January 20, 2016	June 22, 2016	154
February 20, 2017	June 9, 2017	109
January 25, 2018	June 1, 2018	127
Water level rises above ground surface	**Water level drops below ground surface**	**Days of standing water**
January 4, 2015	August 23, 2015	231
January 2, 2016	August 6, 2016	217
January 31, 2017	August 27, 2017	208
January 5, 2018	June 29, 2018	175

Table.A.3 Spreadsheet processing the spill and seepage data to calculate yearly surface outflow.

Average Spill days	**Average Days of Water within the Fen**	**Flow of oulet using channel dimentions (m^3/s)**	**Flow of outlet using hardwater buildup levels (m^3/s)**	**Flow of Seepage (m^3/s)**	**Total Spill using channel data (m^3/yr)**	**Total Spill using circular weir (m^3/yr)**	**Total Seepage (m^3/yr)**	**Average of Both Spill Approximations (m^3/yr)**	**Total Runnoff (m^3/yr)**

136	208	0.00114	0.0013	0.00013	13426	15266	2330	14346	16676

Table.A.4 The table below lists values associated with the pan-coefficient, and suggests a value for evapotranspiration using said coefficient. The new ET value assumes that half of the year is pond (experiencing pan evaporation) while half of the year is similar to a green cropped area (experiencing near reference ET values).

Average Wind Speed (m/s)	**RH %**	**Distance from Drier Area (m)**	**Reference ET from Davis weather station (mm/yr)**	**Pan coefficient**	**Fen ET value (mm/yr assuming 50% pond conditions)**
1.81	41	85	1162	0.8	1307.25

Table.A.5 The chart below expresses the water level change and recharge associated with a rain event. The lowest recorded water table measurement is used to calculate the added precipitation necessary for a standing-water condition.

Water Levels before and after event (mm)		Change in Water Level (mm)	Recharge (mm)	Specific Yield	Hydrograph Minimum (m) according to ground level	Precipitation Needed to bring water table to ground level during minimum scenario (m)
693	764	71	19.3	0.272	-0.630	2.318

Table.A.6 The table below describes the methodology in calculation PJ transpiration using hydrograph measurements, tree-canopy measurements from satellite imagery, and daily transpiration values (Bedell et al., 1993). The table below calculates the added precipitation necessary to satisfy the PJ forest enough for standing water (pond) conditions. Note that changing the first row values can calculate transpiration for any period of time.

Finding the days of decline (below fen surface)	Decline goes beneath ground level	8/30/2015	8/10/2016	8/31/2017			
	Decline End	10/6/2015	12/20/2016	12/21/2017			
	Days of Decline	37	132	112			
	average days of decline (below Surface)	94					
Finding the average area of an adult tree (using the area of the largest trees in the images studied)	Larger (Adult) Single Tree canopy Diameters (m)	7.5	6.6	7.3	5.4	6.25	4.81
	Tree Area m^2	44.2	34.2	41.9	22.9	30.7	18.2
	Average Adult Tree Area (m^2)	32.0					
Calculating tree density from satellite imagery	Images taken from google earth (55x34m)	treez3	treez4	treez5			
	Area of tree canopy (MATLAB; m^2)	1184.8	1395.5	1415.7			
	# of trees	37.0	43.6	44.2			

	Density (m^2/tree)	50.5	42.9	42.3
	Area of watershed m^2	990000		
Finding Transpiration for the days of decline (below fen surface). Daily transpiration of adult tree taken from Bedell (1993)	Trees in watershed	19601.7	23087.6	23421.8
	m^3/day (low bound)	0.075		
	m^3/day (high bound)	0.15		
	mm of transpiration (low bound)	139.1	163.8	166.2
	mm of transpiration (high bound)	278.2	327.7	332.4

Table.A.7 Sedimentation rates recorded in GBC2.

Depths (cm)	**Sedimentation Rate (cm/yr)**
0-24	0.0612
24-51	0.0123
51-123	0.0140
123-157	0.0168
157-282	0.0842

Due to the tens of thousands of data points from the weather station, piezometer, thermistors, and pyrolysis study, not all information was listed in this study. A digital archive has been created with this data, as well as over a hundred images from ESEM, trail camera, and other devices.